Water and Desalination Research Journal
Vol. 3, No. 1; 2019
Published by CanSRG
http://cansrg.com/journals/drj/

Role of surface chemistry and textural characteristics of ACs from coffee and cocoa seed husks biomass in the adsorption of Ni and Co ions

Mónica Hernández Rodríguez[a,c], Jan Yperman[b*], Robert Carleer[b], José Falcón Hernández[c], Alexis Otero Calvis[a], Grazyna Gryglewicz[d], Katarzyna Chomiak[d]

[a]*Mineral and Metallurgic Institute (ISMM), Moa, Holguín, Cuba.*
[b]*Research group of Applied and Analytical Chemistry, Hasselt University, Agoralaan building D, 3590-Diepenbeek, Belgium.*
[c]*Faculty of Chemical Engineering, Universidad de Oriente, Santiago de Cuba, Cuba.*
[d]*Department of Polymer and Carbonaceous Material, Faculty of Chemistry, Wroclaw University of Technology, Gdanska 7/9, 50-344 Wroclaw, Poland.*

Abstract

The aim of this research is to relate surface chemistry and textural characteristics of activated carbons (ACs) in the adsorption of Ni and Co ions present in single, bi and multi-element solutions, which simulates the wastewater from an acid leaching mineral processing technology. The chars were treated with Na_2S solution before activation process for pore development. Batch adsorption test were done as a function of heavy metal concentration, adsorbent doses, temperature and adsorption time. The adsorption behaviour was evaluated through isotherm models, thermodynamics and kinetics parameters. At 25ºC Langmuir maximum adsorption capacity (q_m) for Ni and Co ions is higher for the ACs without chemical pre-treatment. The adsorption of the metallic species is endothermic and spontaneous in nature, with the combination of physical and chemical forces. Both surface functionalities and contribution of mesopores affect the kinetics. However the rate-controlling step is chemisorption and their behaviour is explained by a "surface enhancement" associated with highly energetic and heterogeneous surface. In multi-element solutions containing Ni(II), Co(II), Mn(II) and Mg(II) ions, the adsorption is enhanced for ACs with better developed mesoporosity.

Keywords: *Adsorption, Ni(II); Co(II); coffee husks; cocoa seed husks.*

1. Introduction

Nowadays the increase of heavy metals in the environment is a major concern, for their toxicity and propensity to bio-accumulate in the food chain. They can cause harmful effects to the flora, fauna and humans even at low concentrations [1].

The main sources of heavy metal pollution are industrial growth and human activities [2]. Nickel and cobalt are technologically important and commonly used heavy metals [3, 4]. The excessive levels of nickel in the environment can cause pulmonary fibrosis, lung cancer, renal oedema, skin dermatitis and inhibit many enzymatic functions [4, 5], while cobalt causes paralysis, diarrhoea, low blood pressure, lung irritation and bone defects [6]. Several industries, such as electroplating, ceramics, pigments, electronic, nonferrous metals mineral processing, dyeing and steam-electric power plants have contributed to the contamination of different water bodies with nickel and cobalt ions [7, 8].

* Corresponding author; email: jan.yperman@uhasselt.be
Submitted: September 2, 2019 Accepted: October 13, 2019

Standard levels of nickel and cobalt ions in drinking water are 0.07 mg/L [9] and 0.05 mg/L [6], respectively. Mineral processing using acid leaching technology leaves about 40-45 mg/L of nickel(II) and 5 mg/L of cobalt(II) in the aquatic environment. The waste that contain these elements also has high quantities of manganese(II) and magnesium(II), making the recovery of nickel(II) and cobalt(II) a complex process. Therefore, the development of effective methods for nickel(II) and cobalt(II) recovery from these industries effluents is a challenging situation.

Activated carbon (AC) is very effective in treating low metal-ion concentration in aqueous solutions [10-14]. The use of agricultural waste as AC precursors is renewable, less expensive and offers environmental advantages [15]. There have been many efforts to obtain low-cost AC from agro-waste such as tobacco residues [16], cocoa shells [17], coffee husks [18-20], olive stones, bagasse, birch wood [21, 22], almond shells [23], nut shells [24], rice hulls [25], bamboo [26, 27], tamarind wood [28] and others [29].

ACs application in adsorption process is mostly related with their surface chemistry and pore structure [30, 31]. Thus, the main purpose of researches in the last years is to obtain ACs with specific surface functionalities and/or to improve the micro and mesoporosity of the adsorbents [30, 32], through surface modification using techniques such as: acid or base treatment, impregnation with several chemical reagents and thermal processes [31, 33-35]. The chemical treatment of chars prior to activation produces more active sites into their structure, which afterwards can improve micro- and mesopore development during steam activation [30, 36, 37]. Pore structures enhance the AC adsorption capacity, where mesopores have a significantly role acting as the main transport routes for the adsorbate to the micropores [36, 38]. However, little or no information is known concerning the relation of chemical and textural characteristics of AC from coffee and cocoa seed husks pre-treated with Na_2S in the adsorption of Ni and Co ions.

In this research, ACs are obtained by physical activation of chars from coffee and cocoa seed husks. The chars were pre-treated with Na_2S solution to increase ACs pore structure development and to modify their surface functionalities. Adsorption processes of Ni and Co ions present in single, bi and multi-elemental solutions are evaluated. Adsorption models (Langmuir, Freundlich and Langmuir-Freundlich), thermodynamics, kinetics and characteristics of the adsorbent materials are also assessed.

2. Materials and methods

2.1. Chemicals and solutions for adsorption processes

All reagents used were analytical grade and purchased from Merck. Stock solutions of 5000 mg/L for Ni(II), Co(II), Mn(II) and Mg(II) were separately prepared by dissolving $NiSO_4 \cdot 6H_2O$, $CoSO_4 \cdot 7H_2O$, $MnSO_4 \cdot H_2O$ and $MgSO_4 \cdot 7H_2O$ in Milli-Q water. All other solutions containing these metals ions were prepared by diluting the stock solutions. The pH of the solution was adjusted with 0.1 N NaOH or 0.1 N HCl solutions. The concentration of metal ions was determined using an inductively coupled plasma spectrophotometer (Perkin Elmer Optima 3000 DV ICP-AES device with an axial plasma configuration).

2.2. Raw materials, preparation of activated carbons

In reference [39 and 40] a detailed description of the preparation of both biochars is given using an own build reactor.

For activation, the biochar is introduced in a horizontal quartz reactor and fixed with two quartz wool plugs. The biochar is heated up under a N_2 atmosphere at 850°C with a heating rate of 20°C/min. At 850°C the atmosphere is switched from N_2 to water vapour (10 mL) to

complete the activation process during 30 min and 39 min for coffee husk char and cocoa seed char [40], which were denoted as HAC and CAC respectively.

For the preparation of pre-treated ACs 8 g of biochar is mixed with 50 mL of 0.1 N $Na_2S{\cdot}9H_2O$ solution and dried overnight at 110°C until the complete evaporation of the solvent. Then, the impregnated biochar is thoroughly washed with Milli-Q water, dried at 110°C for 24 h and conducted to activation process. The chemical pre-treated coffee and cocoa seed husks AC were coded as S-HAC and S-CAC respectively.

2.3. Characterization of adsorbent materials

In reference [40] the porous texture analysis methods using N_2 and CO_2 are described and the calculation of the different parameters: micropore volume ($V_{DR,N2}$) and average micropore size ($L_{0,N2}$), mesopore volume (V_{Mes}), total pore volume (V_T), ultramicropore volume ($V_{DR,CO2}$) and ultramicropore size ($L_{0,CO2}$), and pore size distribution (PSD) is according references [41-44].

The content of the mineral matter soluble in acid was performed by leaching 100 mg of the AC samples with 0.1 N HCl solution for 48 h. The solution was filtrated and the concentration of K, Na, Ca and Mg was measured using inductively coupled plasma spectrophotometer (Perkin Elmer Optima 3000 DV ICP-AES device with an axial plasma configuration). The composition of the overall mineral fraction was determined by XRF (X-Ray Fluorescence). XRF analysis was executed on a Bruker S4 Explorer (wavelength dispersive XRF spectrometer, 1000 W). Powdered samples were measured in a He atmosphere. The observed intensities of the analyzed samples were compared to a set of universal calibration standards (standard less calibration). The concentration of the elements in the samples (in %) was obtained applying a correction for the sample matrix (by the amount of carbon present) and using the EVAL-program for this purpose.

The pH determination at zero charge (pH_{PZC}) was determined by acid-base titration procedure [45]. In brief, 50 mL of a 0.01 N NaCl solution was adjusted between pH 2 and 12 with the addition of a solution of 0.01 N HCl or 0.01 N NaOH in different flasks, 0.15 g of AC sample was added to each flask and shaken for 48 h. The final pH was measured. The pH_{PZC} value is the point where the curve pH_{final} versus $pH_{initial}$ crosses the line $pH_{initial} = pH_{final}$.

ATR-FTIR measurements were performed to assess the functional groups involved in the adsorption mechanism. The dried samples were directly measured in the wavenumber range from 4000 to 600 cm^{-1} with a resolution of 4 cm^{-1} using a Bruker Vertex 70 equipped with a DTGS detector (32 scans) and diamond ATR crystal.

The number of total acidic groups was determined according to the Boehm titration method. The adsorbent (1.0 g) was added to 50 mL of the following solutions: NaOH (0.05 N), Na_2CO_3 (0.05 N) and $NaHCO_3$ (0.05 N). The method is based on the theory that NaOH neutralizes carboxyl, lactone and phenolic groups, Na_2CO_3 carboxyl and lactone groups, and $NaHCO_3$ only neutralizes carboxyl groups [46]. The flasks were sealed and shaken for 24 h. Subsequently, 10 mL of each filtrate was pipetted, the excess of the base or acid was titrated with HCl (0.05 N) or NaOH (0.05N) to a pH of around 7.

The surface elemental compositions of ACs were determined by X-ray photoelectron spectroscopy (XPS) using a PHI 5000 VersaProbe spectrometer. The XPS spectrum was calibrated with respect to the C1s signal at 284.5 eV. Curve fitting was performed by an iterative least-squares algorithm (CasaXPS software) using a Gaussian-Lorentzian (70/30) peak shape and applying the Shirley background correction.

Elemental analysis of carbon (C), nitrogen (N), hydrogen (H) and sulphur (S) was carried out with a Thermo Electron Flash EA1113 element analyser with BBOT (2,5-bis(5-tert-butyl-benzoxazol-2-yl) thiophene with formula $C_{26}H_{26}N_2O_2S$) as standard for calibration.

The proximate analysis was determined according to ASTM test methods. Moisture content of the samples was determined according to ASTM 1756-01 [47] by oven drying the sample at a temperature of 105±3 °C until constant weight. Volatile matter by ASTM D 3175-17 [48] is the percentage of volatile products, exclusive of moisture vapor, released during the heating of AC (around 1 g) at 950±25 °C for 7 minutes. Ash content was determined by ASTM E 1755-01 [49] by dry oxidation of the sample at 575±25 °C for a minimum of 3 h. Fixed carbon is the non-volatile fraction and is determined by difference. The analyses were performed in quadruplicate.

The granulometric characteristics of adsorbent materials were obtained at the size intervals (in mm) $>$ 2; 2-1; 1-0.5; 0.5-0.125; 0.125-0.063 and $<$ 0.063. For adsorption tests the particles with the size distribution $<$ 0.063 were neglected.

2.4. Effect of metal ion concentration

Adsorption tests, for evaluating the initial concentration of Ni(II) and Co(II) on AC adsorption capacities, were carried out at 25ºC in an Erlenmeyer of 250 mL. The amount of adsorbent (25 mg) was added to a 50 mL of Ni(II) or Co(II) solution with metal ion concentration between 30-180 mg/L and solution pH of 6. All experiments were performed during 24 h of contact time. After each experiment, the solution was filtered using a Ø 150 mm filtration paper, the final pH and the concentration of metal ions were determined.

The amount of Ni(II) or Co(II) adsorbed q_e (mg/g) at equilibrium, was calculated using the following equation.

$$q_e = \frac{C_0 - C_e}{m} \times V \quad (1)$$

where c_0 and c_e are the initial and equilibrium concentration of metal ions, respectively (mg/L); m (mg) the mass of AC and V(L) the volume of the solution. The real value of c_e (Equation. 2) was corrected taking into account the amount of Ni(II) or Co(II) that precipitated in the solution because of the increase of the pH. When the pH increases over 7.5, an additional measurement was performed using an Erlenmeyer containing 50 mL of metal ion solution (ion concentration used during the adsorption test run) and shaken at 50 rpm. Diluted solutions of 0.1 N HCl or 0.1 N NaOH were added to this solution until the same pH was reached as in the case of the adsorption experiment. Then the solution was filtrated, and the ion concentration was measured. The amount of metal ions that precipitate was determined by the difference between initial and final concentration, taking into account the corrections by the volume of added acid or base. This procedure was applied for all adsorption tests: temperature, adsorbent doses effect, kinetic and adsorption in multi-element solution.

$$C_e = C_{e\,measured} + C_{precipitated} \quad (2)$$

where $C_{e\,measured}$ is the filtrated metal ion concentration after the adsorption test and $C_{precipitated}$ is the precipitated metal ion concentration determined according to the procedure described above.

The removal percentage of adsorbed heavy metals was estimated by:

$$R_{emoval}(\%) = \frac{C_0 - C_e}{C_0} \times 100 \quad (3)$$

2.5. Adsorption isotherms

The analysis of the equilibrium data is essential to study the adsorption behaviour. Freundlich, Langmuir and Langmuir-Freundlich models were fitted to adsorption data.

The Freundlich isotherm is an empirical model and can be applied to multilayer adsorption, with non-uniform distribution of adsorption, heat and affinities over the heterogeneous surface [50, 51] and in linear form it is given by

$$\log q_e = \log K_F + \frac{1}{n}\log C_e \quad (4)$$

where K_F is related with the adsorption capacity ($mg^{1-1/n}L^{1/n}g^{-1}$) and *n* is related to the heterogeneity and the adsorption intensity [50].

The Langmuir isotherm is based on a theoretical model and assumes a monolayer adsorption over an energetically homogeneous adsorbent surface containing a finite number of adsorption sites. It does not take into account interactions between adsorbed molecules/ions [52, 53]. It can be represented by the following linear equation

$$\frac{1}{q_e} = \frac{1}{q_m} + \left(\frac{1}{K_L q_m}\right)\frac{1}{C_e} \quad (5)$$

where q_m and K_L are constants referring to the maximum adsorption capacity (mg/g) and related to the adsorption energy (L/mg), respectively. Hereby, a dimensionless constant, known as separation factor (R_L) [54] can be defined by

$$R_L = \frac{1}{1+K_L C_0} \quad (6)$$

The R_L value indicates the adsorption nature to be either unfavourable (R_L >1), linear (R_L =1), favourable (0 <R_L <1) or irreversible (R_L =0) [55].

The Langmuir-Freundlich isotherm equation [56] represents the combination of Langmuir and Freundlich behaviour through

$$q_e = \frac{q_{m_{LF}}(K_{LF}\, c_e)^{n_{LF}}}{(K_{LF}\, c_e)^{n_{LF}}+1} \quad (7)$$

where q_{mLF}, K_{LF} and n_{LF} refer to the maximum adsorption capacity (mg/g), the adsorption energy (L/mg) to the adsorption intensity for Langmuir-Freundlich model respectively. To determine the parameters of the model nonlinear curve fitting was applied to the data using the Origin 8.1 program.

2.6. Temperature effect

The effect of temperature in the adsorption process was evaluated in the range of 25-45ºC. The adsorbent (25 mg) was added to a 50 mL of Ni(II) or Co(II) solution with metal ion concentration between 30-180 mg/L in an Erlenmeyer of 250 mL and at a solution pH of 6. The Erlenmeyers were sealed and shaken during 24 h. After agitation, the adsorbent was removed by filtration and 10 mL of solution was taken to determine the concentration of metal ions.

2.7. Effect of adsorbent doses

Solutions of Ni and Ni plus Co ions were prepared, the last simulating the concentration of these metals in wastewater of the acid leaching process. The effect of adsorbent doses was carried out using batch adsorption experiments in Erlenmeyer of 250 mL. The amount of adsorbent, between 25-50 mg, was added to the Erlenmeyer containing 50 mL of solution for achieving a solid/liquid ratio in the range 0.5-1.0 g/L, at temperatures between 25-45ºC and at a solution pH of 6. The Erlenmeyer was sealed and shaken during 24 h. After agitation, the

adsorbent was removed by filtration and 10 mL of solution was taken to determine the concentration of metal ions.

2.8. Thermodynamics and kinetics parameters

The free energy change ($\Delta G°$), enthalpy change ($\Delta H°$), and entropy change ($\Delta S°$) of the adsorption process were determined and can be obtained from [57, 58]

$$\ln K_e = \frac{\Delta S°}{R} - \frac{\Delta H°}{RT} \quad (8)$$

$$\Delta G° = -RT\ln K_e \quad (9)$$

where K_e is the equilibrium constant. The values of ΔH° (kJ/mol) and ΔS° (J/molK) can be calculated, respectively from the slope and intercept of $\ln K_e$ versus 1/T plot.

According to Liu [59], for an adsorption process described as follows.

$$A + B \leftrightarrows AB \quad (10)$$

where A is the free adsorbate molecules, B is the vacant sites on the adsorbent, and AB the occupied sites. K_a is defined as [59].

$$K_a = \frac{(\text{activity of occupied sites})}{(\text{activity of vacant sites})(\text{activity of solute in solution})} = \frac{a_{AB}}{a_B \cdot a_A} \quad (11)$$

Considering that the activity coefficients of the occupied and vacant sites are the same, Equation. 11 becomes

$$K_a = \frac{\theta_e}{(1-\theta_e)\gamma_e C_e} \quad (12)$$

where θ_e is the fraction of the surface covered at equilibrium, $\theta_e = q_e/q_m$ and γ_e is the activity coefficient of the adsorbate in the solution at equilibrium [59]. Considering a dilute solution ($\gamma_e = 1$) the equilibrium constant can be rewritten as

$$K_a = \frac{q_e/q_m}{\left(1-q_e/q_m\right)C_e} \quad (13)$$

Rewriting the linear form of the Langmuir equation (Equation. 5), one gets

$$\frac{q_e}{q_m} = \frac{K_L C_e}{K_L C_e + 1} \quad (14)$$

For the charged adsorbate (Ni and Co ions), the effect of ionic strength can be neglected because of using diluted solutions. As a consequence, the equilibrium constant K_e can be defined as K_a and substituting Equation. (13) in (12) equals to the Langmuir constant (K_L). To get a dimensionless equilibrium constant K_L must be multiplied with 1000 and by the atomic weight of the considered adsorbate. Subsequently the thermodynamic parameters obtained via Equation. 8 and 9 in using K_L must be considered as an approximation of the thermodynamic effects.

The characteristics of the kinetic process allow understanding the adsorption mechanism. The pseudo first-order rate equation of Lagergren is a commonly used kinetic model depending solely on the adsorbate concentration in the evaluation of adsorption mechanism of the solute from a liquid solution [60]. The pseudo-second order kinetic model is based on the assumption that the rate-limiting step is chemisorption in nature and the mechanism could involve valence forces by sharing or through the exchange of electrons between adsorbent and adsorbate [1]. Linearized models can be expressed for the following equations [61]

$$log(q_e - q_t) = \log q_e - \frac{k_1}{2.303} t \quad (15)$$

$$\frac{t}{q_t} = \frac{1}{k_2 q_e^2} + \frac{1}{q_e} t \quad (16)$$

Where k_1 and k_2 are the adsorption rate constants of first and second order kinetic models, in min^{-1} and g/(mg min), respectively; q_e and q_t, in mg/g, are equilibrium adsorption capacity at equilibrium time and at time t. From the slope and the intercept of each linear plot, the adsorption rate constants (k_1 and k_2) can be calculated.

2.9. Activation Energy

Arrhenius equation allows to determinate the activation energy (E_a) throughout the linearized equation [62]

$$\ln k = \ln A - \frac{E_a}{RT} \quad (17)$$

where k the rate constant value for the metal adsorption, A is the frequency factor related with the possibility that the collisions are favourably oriented for reaction, E_a is the activation energy in kJ/mol, T the absolute temperature (K) and R the universal gas constant (8.314 J/mol K). The value of E_a can be estimated by the slope of graph ln k vs 1000/T.

2.10. Adsorption test in multi-element solutions

A multi-element solution containing Ni(II), Co(II), Mg(II) and Mn(II) ions was prepared. The concentration of the metal ions was similar to the wastewater from the acid leaching mineral processing technology: 40 mg/L of Ni(II), 5 mg/L of Co(II), 1062 mg/L of Mg(II) and 1858 mg/L of Mn(II). The adsorption test in batch mode was done at the optimal temperature in sealed Erlenmeyers of 250 mL containing 50 mL of the multi-element solution, pH 6 and at two different adsorbent doses of 62.5 and 125 mg (1.25 and 2.5 g/L) during 24 h of contact time and at 50 rpm of shake speed. Finally, the adsorbent was separated through filtration and the concentration of metal ions and the final solution pH were measured.

3. Results and discussion

3.1. Characterization of adsorbent materials

Table 1 presents the size distribution for the adsorbent materials. As only during biochar formation the particle size changes, due to the continuous motion of an Archimedes screw, HAC and S-HAC; CAC and S-CAC have the same size distribution (activation was performed in a horizontal static reactor oven keeping samples untouched/motionless). HAC and S-HAC are mainly present as particles between 1-0.5 and 0.5-0.125 mm with 52.15 and 34.34 % wt., respectively. However, for CAC and S-CAC, the main size classes are 2-1 and 1-0.5 mm with 44.42 and 25.32 % wt. respectively.

The values of pH_{PZC} for HAC and CAC are 8.9 and 8.7 respectively. The pH_{PZC} in ACs is down to 7.1 for S-HAC and 6.5 for S-CAC. The elemental, proximate, overall mineral fraction, surface atomic composition and Boehm titration results of adsorbent materials are shown in Tables 2-4. Chemical pre-treatment with Na_2S leads to a decrease in oxygen content, moisture, ash and volatile compounds, and increasing the total and fixed carbon (Table 2). The amount of sulphur determined by the elemental analysis technique is below detection limit for all samples (Table 2).

XRF results (Table 3) expressed as elements show an increase in sulphur and sodium content after the chemical pre-treatment. The content of sulphur as element is 0.33 %, 0.39 %, 0.80 % and 0.58 % for HAC, CAC, S-HAC and S-CAC, respectively. The content of sodium as element is 0.11 %, 0.19 %, 2.35 % and 2.76 % for HAC, CAC, S-HAC and S-CAC,

respectively. High contents of Mg, Si, P, K and Ca were also found in the ACs samples (Table 3).

Table 1. Size distribution of HAC, S-HAC, CAC and S-CAC.

Size distribution (mm)	% wt. of dry sample	
	HAC & S-HAC	CAC & S-CAC
> 2	0.18	6.17
2 - 1	11.73	44.42
1 - 0.5	52.15	25.32
0.5 - 0.125	34.34	19.69
0.125 - 0.063	1.41	3.70
< 0.063	0.19	0.70
Total	100	100

Table 2. Elemental and proximate composition.

Adsorbent materials	Elemental composition (wt. %)					Proximate analysis (wt. %)			
	C	H	N	S	O*	Moisture	Volatile	Ash	Fixed Carbon
HAC	59.30	1.34	0.75	<DL	6.18	5.94	17.84	32.43	43.79
CAC	48.82	1.21	0.84	<DL	5.42	6.02	15.44	43.71	31.83
S-HAC	67.45	1.24	0.77	<DL	4.72	4.12	16.06	25.82	54.00
S-CAC	57.61	1.27	0.95	<DL	3.52	4.10	13.28	36.65	45.97

*by difference: O%=100%-(C+H+N+ash)%; <DL=below detection limit

Table 3. Total mineral matter fraction (based on XRF) expressed as elements and Ca as CaO.

Formula	HAC	CAC	S-HAC	S-CAC
	Element (%)	Element (%)	Element (%)	Element (%)
Na	0.11	0.19	2.35	2.76
Mg	1.88	5.58	2.09	5.22
Al	0.10	0.19	0.11	0.22
Si	1.03	1.17	0.81	1.03
P	0.48	4.89	0.48	4.06
S	0.33	0.39	0.80	0.58
Cl	0.02	0.15	ND	0.03
K	13.80	17.00	6.66	8.13
Ca	9.40	4.35	10.20	3.72
Ti	trace	0.01	trace	0.01
Cr	0.01	trace	0.01	trace
Mn	0.02	0.05	0.02	0.04
Fe	0.21	0.46	0.24	0.42
Ni	trace	0.03	ND	0.03
Cu	0.03	0.04	0.03	0.04
Zn	ND	0.01	0.01	0.02
Br	trace	ND	ND	ND
Rb	0.02	0.02	0.01	0.01
Sr	0.05	0.02	0.05	0.01
Ba	ND	ND	trace	ND
Pb	ND	ND	ND	ND

ND: not detected (<0.01%)

The total amount of acidic groups present in the AC surface decreases after chemical pre-treatment. The contribution to the decrease of the total amount of acidic groups for HAC and CAC in S-HAC and S-CAC is mainly due to the decrease of carboxylic and phenolic groups. For the lactone groups, after Na_2S pre-treatment its content increases for S-HAC vs HAC and results in a small decrease for S-CAC vs CAC (Table 4). The greatest changes found for S-HAC and S-CAC due to the chemical pre-treatment is evidenced by the XPS results (Table 4): decrease in the oxygen atomic composition, C-O and C=O functionalities, and an increase in the carbon atomic composition and the Csp^2 relative concentration. This indicates that the pre-treatment of chars with Na_2S promotes the aromatization during subsequent thermal treatment which is also reflected by the atomic ratio of O/C.

Table 4. XPS from the C1s deconvolution and Boehm titration results.

Adsorbent materials	Acidic groups (mmol/g)				Surface		Relative concentration		
	Carboxyl	Lactone	Phenolic	Total	C	O	Csp^2	C-O	C=O
HAC	0.581	0.095	0.417	1.093	62.9	37.3	78.2	16.3	3.0
CAC	0.774	0.136	0.603	1.513	60.8	39.2	81.4	14.5	2.2
S-HAC	0.321	0.214	0.116	0.651	77.9	22.1	84.8	7.8	2.6
S-CAC	0.293	0.102	0.091	0.486	72.5	27.5	90.5	6.7	1.3

The ATR-FTIR spectrum (Figure 1b) reveals more intense absorption peaks for CAC. For HAC (Figure 1a) the weak bands located at 3639 cm^{-1} correspond with O-H stretching vibrations from isolated hydroxyl groups [63, 64]; 1373 cm^{-1} is characteristic for phenol or tertiary alcohol -OH stretch [65]; the several peaks between 850-610 cm^{-1} can be attributed to alcohol -OH out of plane bends [64, 65]. After the chemical pre-treatment process, the O-H stretching vibration bands are less intense. The appearance of bands at 1251 cm^{-1} and 998 cm^{-1} suggests the conversion of some alcohol to aromatic ethers [66]. CAC has peaks at 3188 cm^{-1} (O-H stretching vibrations from isolated hydroxyl groups) [64], 1511 cm^{-1} (aromatic C=C-C vibration stretches) [64], 1385 cm^{-1} (phenol or tertiary alcohol -OH stretches) [64], 1038 cm^{-1} (primary alcohol C-O stretches) [64, 65], and several peaks among 900-620 cm^{-1} (alcohol -OH out of plane bending) [64, 65]. Chemical pre-treatment of CAC leads to the removal of almost all functional groups, just the band corresponding to primary alcohol C-O stretch is observed.

(a)

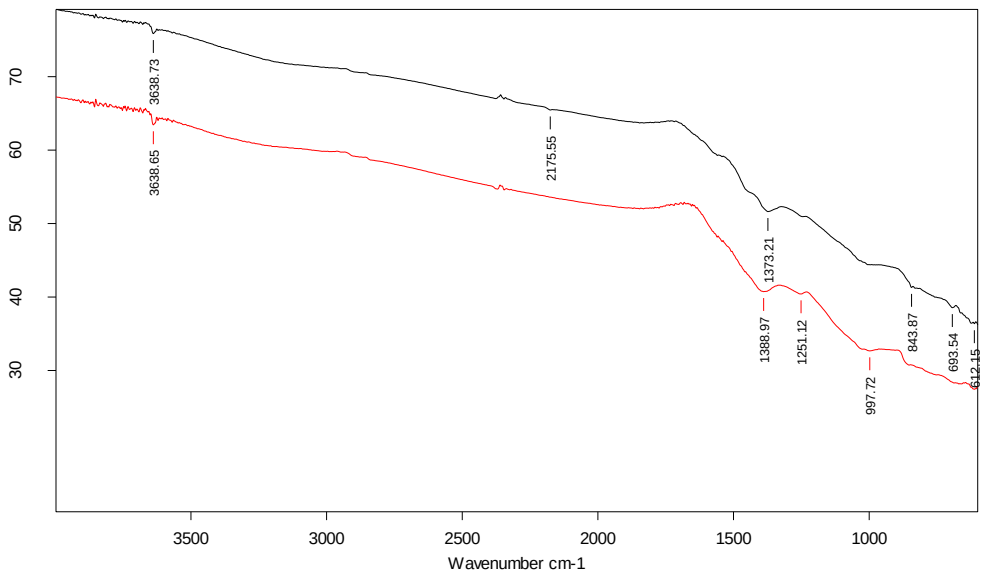

(b)

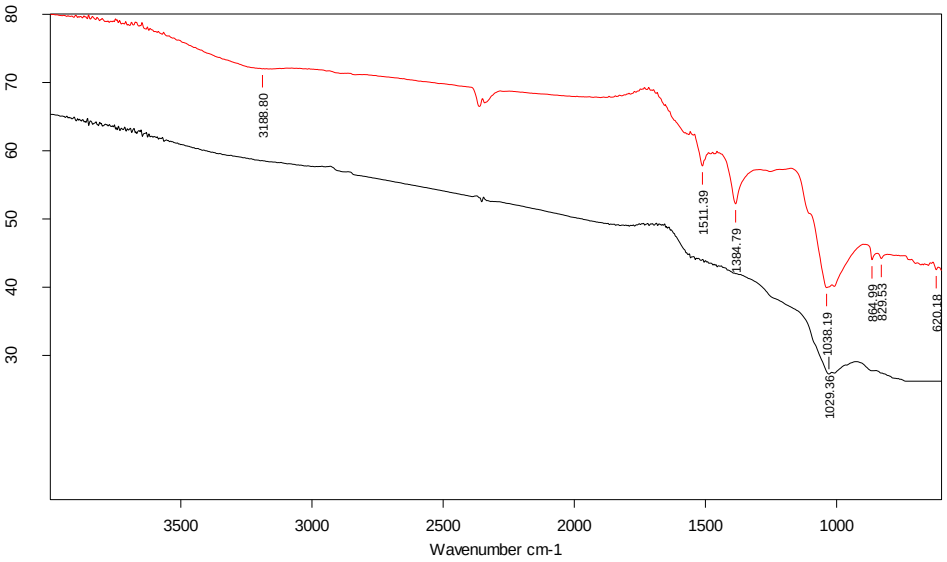

Figure. 1 ATR spectra (a) ── HAC, ──S-HAC, (b) ── CAC, ── S-CAC.

Figure. 2 depicts the nitrogen adsorption-desorption isotherms at -196°C for the studied samples. For CAC the isotherm shape shows a sharply increase at low relative pressure of p/p_0 and reaches a plateau in a broad range of p/p_0. This shape is classified as Type I isotherm, characteristic for microporous materials, having mainly narrow micropores [67]. However, for HAC, S-HAC and S-CAC the isotherm shape continuous increases until the maximum relative pressure. These samples have a combination of Type I with Type IV isotherms, characteristic of microporous and mesoporous materials [67]. The pre-treated S-HAC and S-CAC lead to greater nitrogen uptake at the same value of relative pressure (p/p_0) and more intense hysteresis loops during desorption, usually associated with capillary condensation in the mesopores [67]. The more developed mesoporosity (V_{Mes} and V_{Mes}/V_T ratio), the higher micropore volume (V_{DR}), the larger superficial area (S_{BET}) and the increased total pore volume (V_T) (Table 5) of S-HAC and S-CAC, compared to HAC and CAC, proves that the pre-treatment of chars with Na_2S produces more active sites, which is consequently more developed into micro and mesopores during its steam activation [30]. It is interesting to note that the modification of the chars with Na_2S leads to a decrease in the average micropore size $L_{0,N2}$. Presumably, an increase in the mesopore volume is related to the removal of inorganic constituents occupying mesopores due to the heat treatment with Na_2S. This is confirmed by lower ash content (32.4 vs. 25.8 wt.% for HAC and S-HAC, 43.7 vs. 36.5 wt.% for CAC and S-CAC) in the pre-treated ACs compared to untreated samples (Table 2). In addition, this process increases the volatilization and degradation of organic compounds present at the carbon surface, which is in agreement with lower oxygen, volatile content and a decrease in surface functionalities as indicated by the elemental, proximate analysis, Boehm titration, XPS and ATR-FTIR results (Tables 2 and 4, Figure 1). The pore size distribution determined by QSDFT method confirmed that S-HAC and S-CAC exhibit a more intense maximum at a pore width of 0.57 nm than HAC and CAC (Figure 2b). Other maximum centers are found at 0.79, 1.01, 1.54 nm for CAC; 0.85, 1.68, 3.38 nm for HAC; 1.01, 1.54, 3.70 nm for S-HAC and 1.01, 1.54, 3.38 mm for S-CAC, respectively.

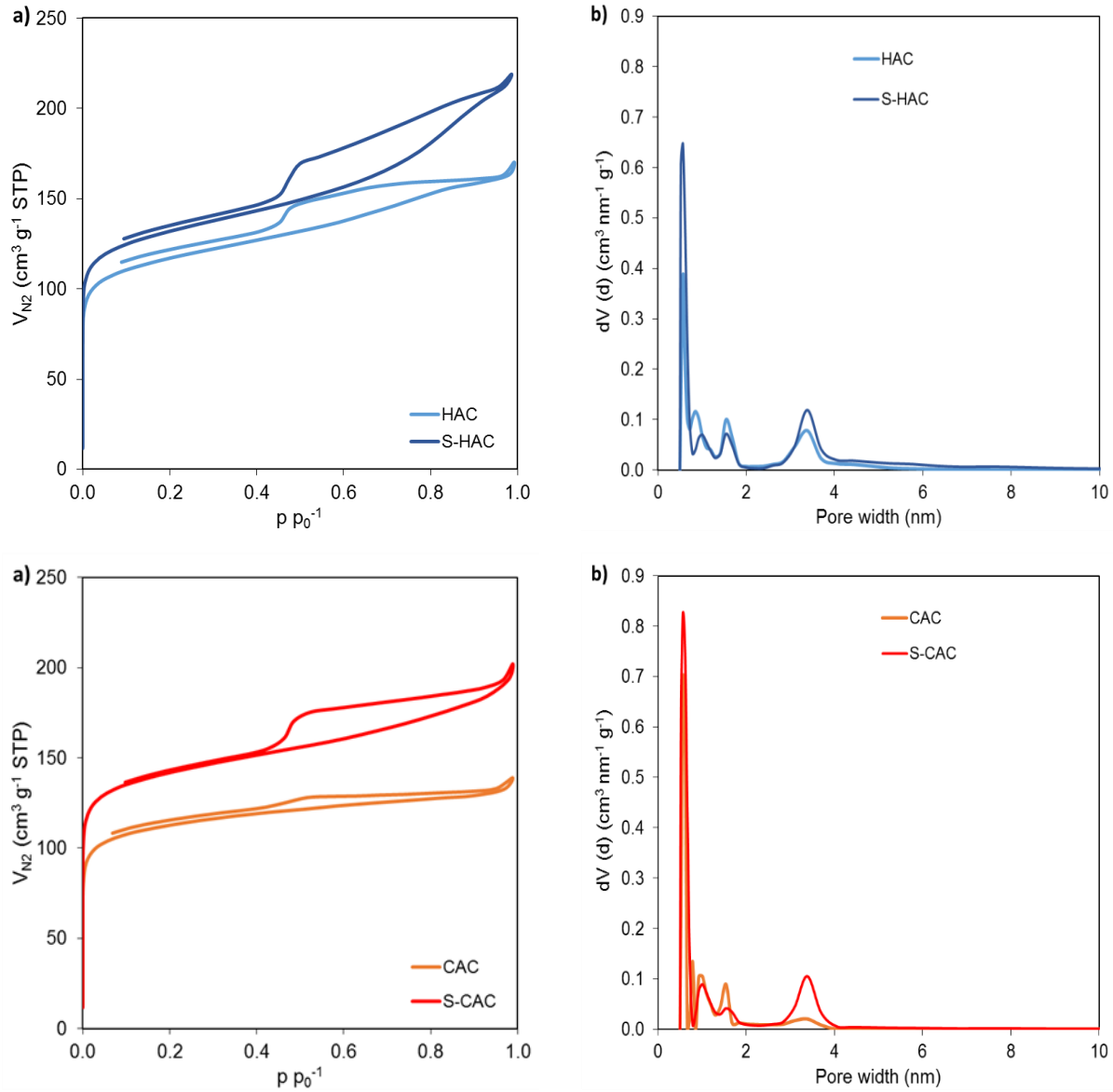

Figure 2. Nitrogen adsorption-desorption isotherms at -196°C (a) and QSDFT pore size distribution (b) for all samples.

Table 5. Textural parameters for HAC, S-HAC, CAC and S-CAC.

Sample	S_{BET} m^2/g	V_T cm^3/g	V_{DR} cm^3/g	V_{Mes} cm^3/g	V_{Mes}/V_T	L_0 nm	$V_{DR,CO2}$ cm^3/g	$S_{0,CO2}$ m^2/g	$L_{0,CO2}$ nm
HAC	438	0.250	0.168	0.082	0.33	0.84	0.166	976	0.34
S-HAC	494	0.326	0.189	0.137	0.42	0.77	0.172	860	0.40
CAC	428	0.204	0.165	0.039	0.19	0.81	0.140	778	0.36
S-CAC	537	0.294	0.205	0.089	0.30	0.74	0.160	800	0.40

The prepared ACs were also analyzed by sorption of CO_2 to characterize ultramicropores. Figure 3 shows the CO_2 adsorption isotherms (a) and the pore size distribution determined by the NLDFT method (b) in the range of ultramicropores. The ACs show a bimodal distribution of ultramicropores size with maximum centers at 0.35 nm and between 0.52-0.55 nm for all samples. The volume and average width of ultramicropores are greater for S-HAC and S-

CAC compared with HAC and CAC. The surface area achieved for the narrow micropores is between 778 - 976 m^2/g (Table 5).

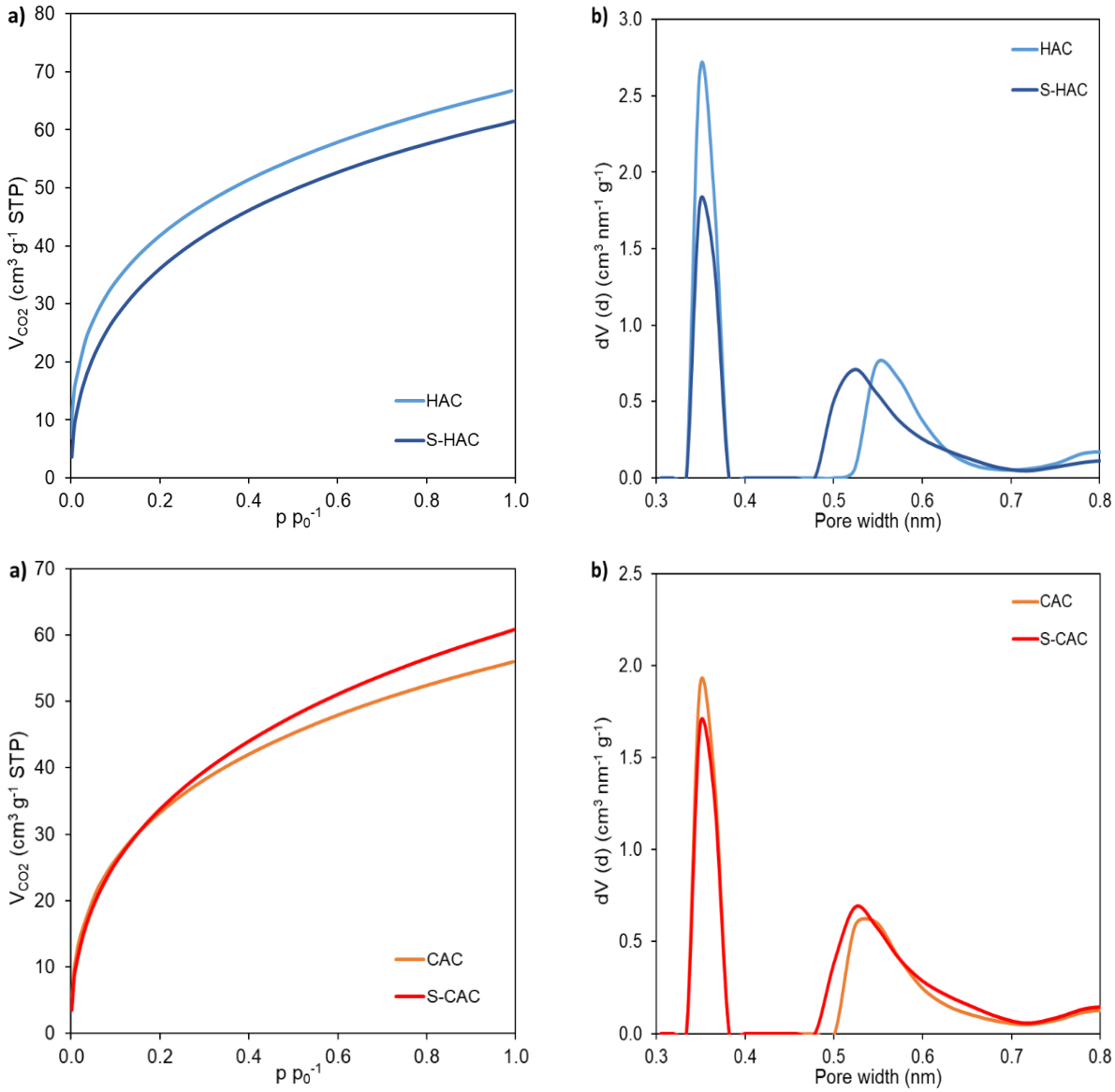

Figure 3. CO_2 adsorption isotherms at 0°C (a) and NLDFT pore size distribution (b) for all samples.

3.2. Effect of initial metal ion concentration

Figure 4 depicts the effect of metal ion concentration on the adsorption capacity and removal % of Ni and Co ions at 25°C. The ACs without chemical pre-treatment (HAC and CAC) perform better than the Na_2S treated, nevertheless their improved surface and pore size characteristics. For these adsorbents, the adsorption capacity increases with initial metal ion concentration and reaches a plateau, achieving values between 80-110 mg/g for both ions. The removal % varies between 85-20% for Ni as a function of the initial concentration and between 76-20% for Co. However, Na_2S pre-treated ACs (S-HAC and S-CAC) show only a slight increase in the adsorption capacity when the initial concentration rises, while the adsorption capacity remains almost constant with values between 30-55 mg/g for Ni and 40-50 mg/g for Co. Removal % in this case decreases with the increasing metal ion concentration from 50-9% for Ni and from 47-11% for Co ions.

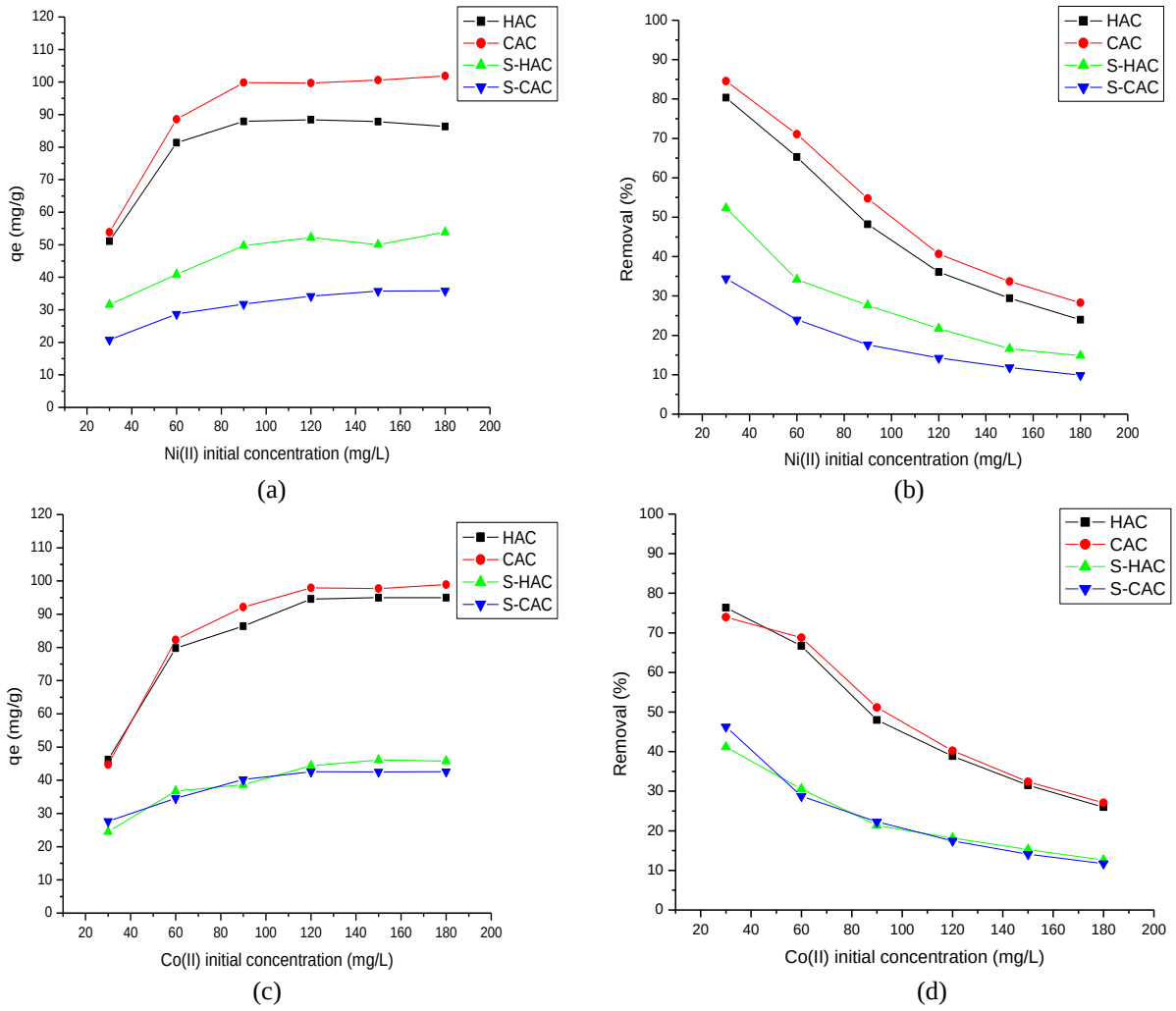

Figure 4. Effect of initial metal ion concentration (a, b) Ni ions, (c, d) Co ions (adsorbent mass = 25 mg, V = 50 mL, initial pH = 6, final pH = 7.7-8.7, T = 25 ºC, shake speed 50 rpm, t = 24 h, particle size class >0.063 mm).

3.3. Adsorption isotherms modelling

Adsorption isotherms modelling is an important step to assess adsorption behaviour. At 25ºC the adsorption data are somewhat better described by the Langmuir-Freundlich model (Table 6), as well for Ni(II) as for Co(II). Only S-CAC for Ni(II) and S-HAC for Co(II) achieved almost the same correlation coefficient for Langmuir-Freundlich and Langmuir models. These results evidence that ACs surface is not completely homogeneous and the adsorption can occur by a monolayer as by a multilayer process. In all cases, the separation factor (R_L) is between 0-1, demonstrating a favourable adsorption process. As already demonstrated by Figure 4, the maximum adsorption capacities (q_m) are higher for CAC and HAC than for S-HAC and S-CAC despite the former ACs have smaller surface area (Table 5), however they have more surface oxygen functionalities (Table 4), being the dominating adsorption factor. These results indicate that at low temperature, adsorption process of ACs from coffee and cocoa seed husks is more related with surface functionalities than with pore structure development.

3.4. Temperature effect

The effect of temperature on Ni and Co adsorption is depicted in Figures 5-6 respectively. From these figures, the positive effect of temperature increase can be noticed but much more for the Na_2S pre-treated ACs. For HAC the impact of the increased temperature on Ni is more

pronounced than for CAC. For Co adsorption nor for HAC nor for CAC a really improved adsorption can be noticed. In the case of S-HAC and S-CAC for Ni as well as for Co a remarkable improvement of adsorption performance can be found. S-HAC and S-CAC reached at 45ºC adsorption capacities around 151 and 134 mg/g for Ni even greater than for HAC and CAC respectively. For Co, 128 and 117 mg/g are found for S-HAC and S-CAC again larger than for HAC and CAC respectively. At 35°C comparable adsorption amounts are found for Ni (123 vs 125 mg/g and 107 vs 108 mg/g) for HAC vs S-HAC and for CAC vs S-CAC. But this is not noticed for Co (101 vs 96 mg/g and 104 vs 88 mg/g), comparing HAC vs S-HAC and CAC vs S-CAC. With the increase of temperature, the impact of surface functionalities seems to decrease in favour of an improved accessibility into the AC structure; S-HAC and S-CAC have higher developed pore volumes, meso- and micropores, than HAC and CAC respectively (see further section 3.6).

Table 6. Isotherm parameters for Ni and Co ions at 25°C.

Carbon	Ni						Co					
	Langmuir		Freundlich		Langmuir-Freundlich		Langmuir		Freundlich		Langmuir-Freundlich	
HAC	R^2	0.9608	R^2	0.774	R^2	0.9948	R^2	0.9738	R^2	0.843	R^2	0.9885
	q_m	92.45	K_F	46.82	q_{mL}	88.24	q_m	101.72	K_F	34.71	q_{mL}	99.10
	K_L	0.259	n	6.378	K_{LF}	0.227	K_L	0.146	n	4.440	K_{LF}	0.148
	R_L	0.021-0.108			n_{LF}	1.696	R_L	0.036-0.184			n_{LF}	1.437
CAC	R^2	0.9898	R^2	0.837	R^2	0.9972	R^2	0.9450	R^2	0.788	R^2	0.9955
	q_m	105.82	K_F	47.34	q_{mL}	102.83	q_m	107.57	K_F	33.07	q_{mL}	98.41
	K_L	0.277	n	5.718	K_{LF}	0.272	K_L	0.128	n	4.057	K_{LF}	0.127
	R_L	0.02-0.102			n_{LF}	1.264	R_L	0.041-0.205			n_{LF}	1.936
S-HAC	R^2	0.9499	R^2	0.931	R^2	0.9538	R^2	0.9748	R^2	0.936	R^2	0.9749
	q_m	57.02	K_F	18.43	q_{mL}	60.54	q_m	51.74	K_F	11.81	q_{mL}	52.20
	K_L	0.086	n	4.548	K_{LF}	0.080	K_L	0.054	n	3.559	K_{LF}	0.053
	R_L	0.060-0.278			n_{LF}	0.810	R_L	0.093-0.383			n_{LF}	0.974
S-CAC	R^2	0.9969	R^2	0.954	R^2	0.9970	R^2	0.9689	R^2	0.947	R^2	0.9739
	q_m	40.01	K_F	10.31	q_{mL}	40.47	q_m	46.03	K_F	16.53	q_{mL}	49.08
	K_L	0.057	n	3.909	K_{LF}	0.056	K_L	0.092	n	5.061	K_{LF}	0.087
	R_L	0.088-0.368			n_{LF}	0.962	R_L	0.057-0.267			n_{LF}	0.780

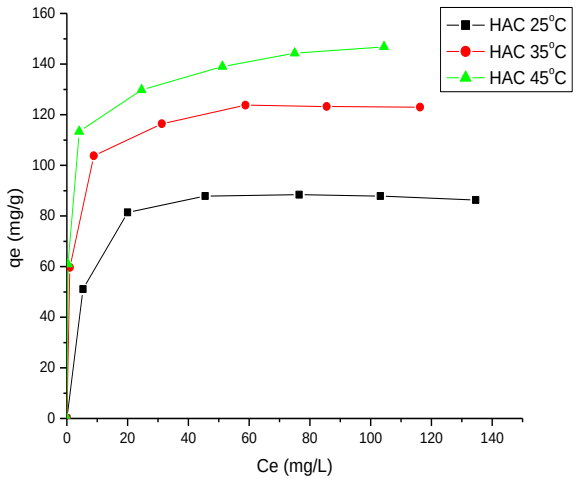

(a)

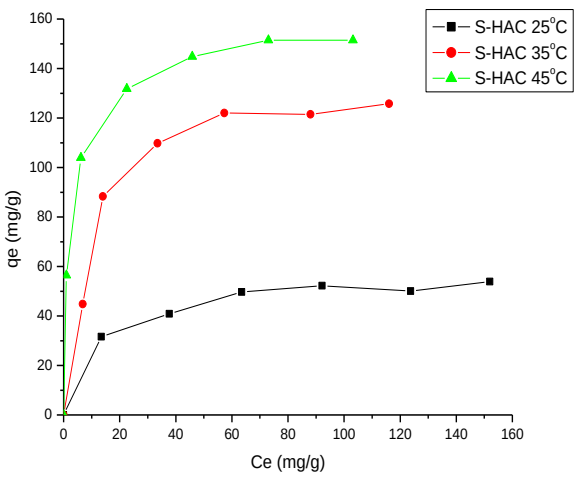

(b)

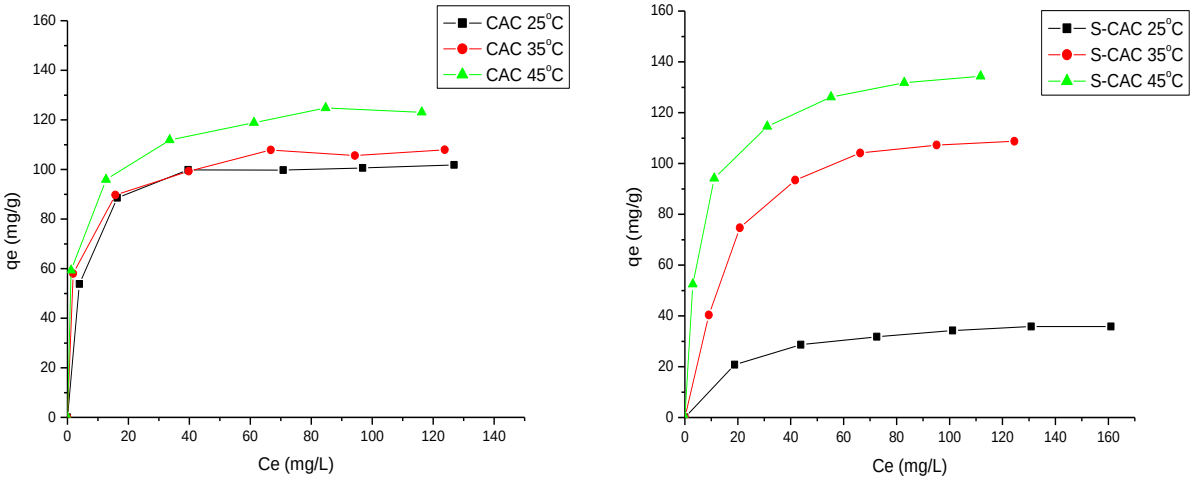

(c) (d)

Figure 5. Effect of temperature for Ni ions (a) HAC, (b) S-HAC, (c) CAC, (d) S-CAC (m = 25 mg, C_0 = 30-180 mg/L, V = 50 mL, initial pH = 6, final pH = 7.5-8.8, shake speed 50 rpm, t = 24 h, particle size class >0.063 mm).

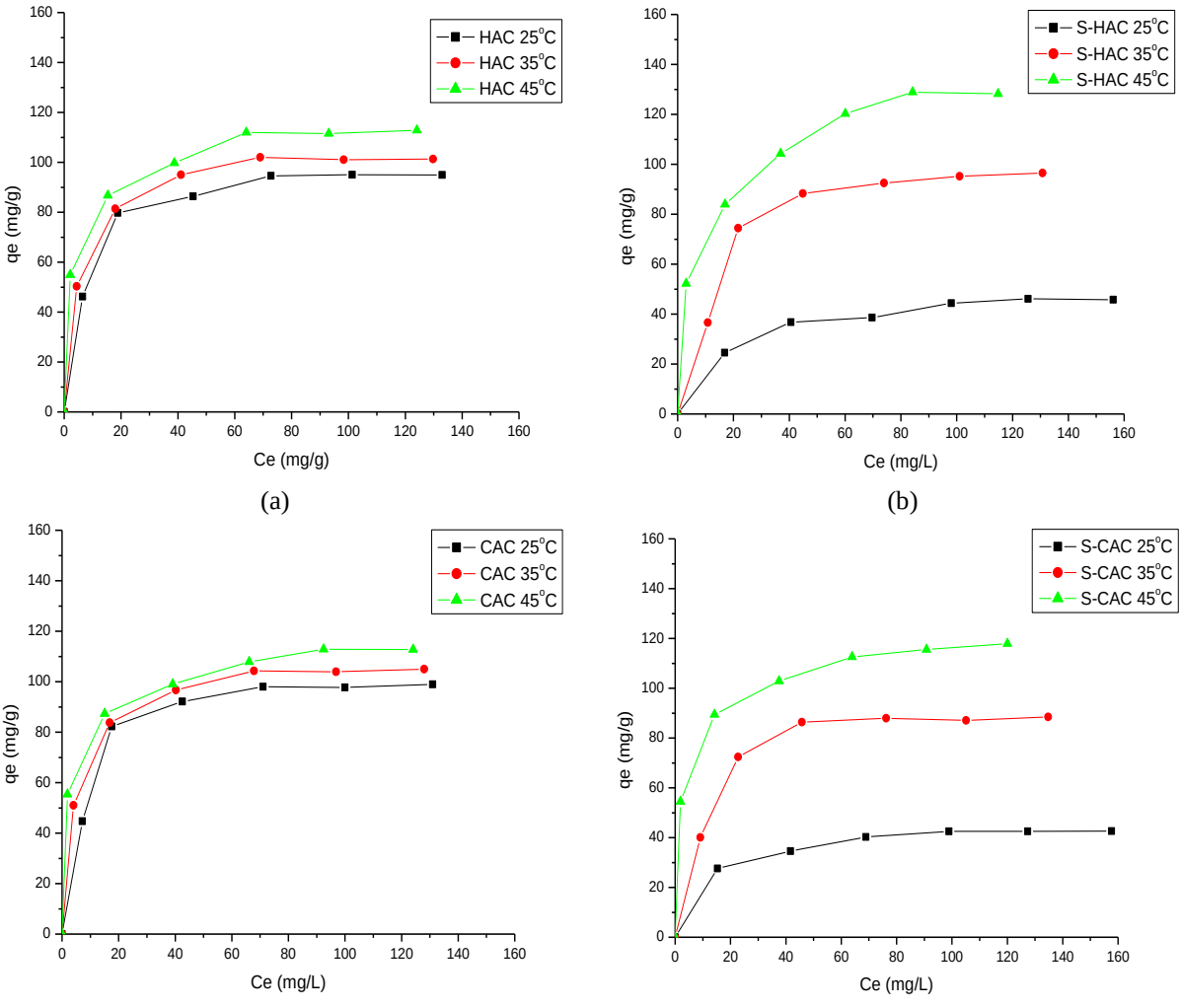

(a) (b)

(c) (d)

Figure 6. Effect of temperature for Co ions (a) HAC, (b) S-HAC, (c) CAC, (d) S-CAC (m = 25 mg, C_0 = 30-180 mg/L, V = 50 mL, initial pH = 6, final pH = 7.5-8.8, shake speed 50 rpm, t = 24 h, particle size class >0.063 mm).

3.5. Effect of adsorbent doses and temperature

The simultaneous evaluation of adsorbent doses and temperature was done for Ni (Figure 7) and combined Ni and Co ion solutions (Figure 8), according to the initial concentration of these species in the wastewater of the industrial acid leaching process. By increasing the adsorbent doses from 25 to 37.5 mg/50 mL, an increment in the removal % of Ni is observed. Further increase in adsorbent doses from 37.5 to 50 mg/50 mL (0.75-1.0 g/L) has no impact for HAC and CAC samples, whatever the working temperature (25-45°C) is. However for S-HAC and S-CAC at 25°C a sharp increase in Ni removal % can be noticed by increasing the adsorbent doses from 25 to 50 mg/50 mL, both for single Ni solution and for the Ni-Co mixtures. This sharp increase in Ni removal % at 35°C and 45°C is only noticed by increasing the adsorbent dose from 25 to 37.5 mg/50 mL; further increase in adsorbent dose from 37.5 to 50 mg/50 mL has for S-HAC and S-CAC no further impact. For all studied adsorbents the best performance is found at 37.5 mg/50 mL and 45ºC. Under these conditions, Ni and Co ion concentrations left in the solution are between 0.2-0.1 mg/L for Ni and lower than 0.01 mg/L for Co, achieving safe discharge standard levels for Co but not for Ni [6, 9]. Removal % higher than 94% of Ni(II) (Figures 7-8) and 98% of Co(II) (Table 7) were achieved.

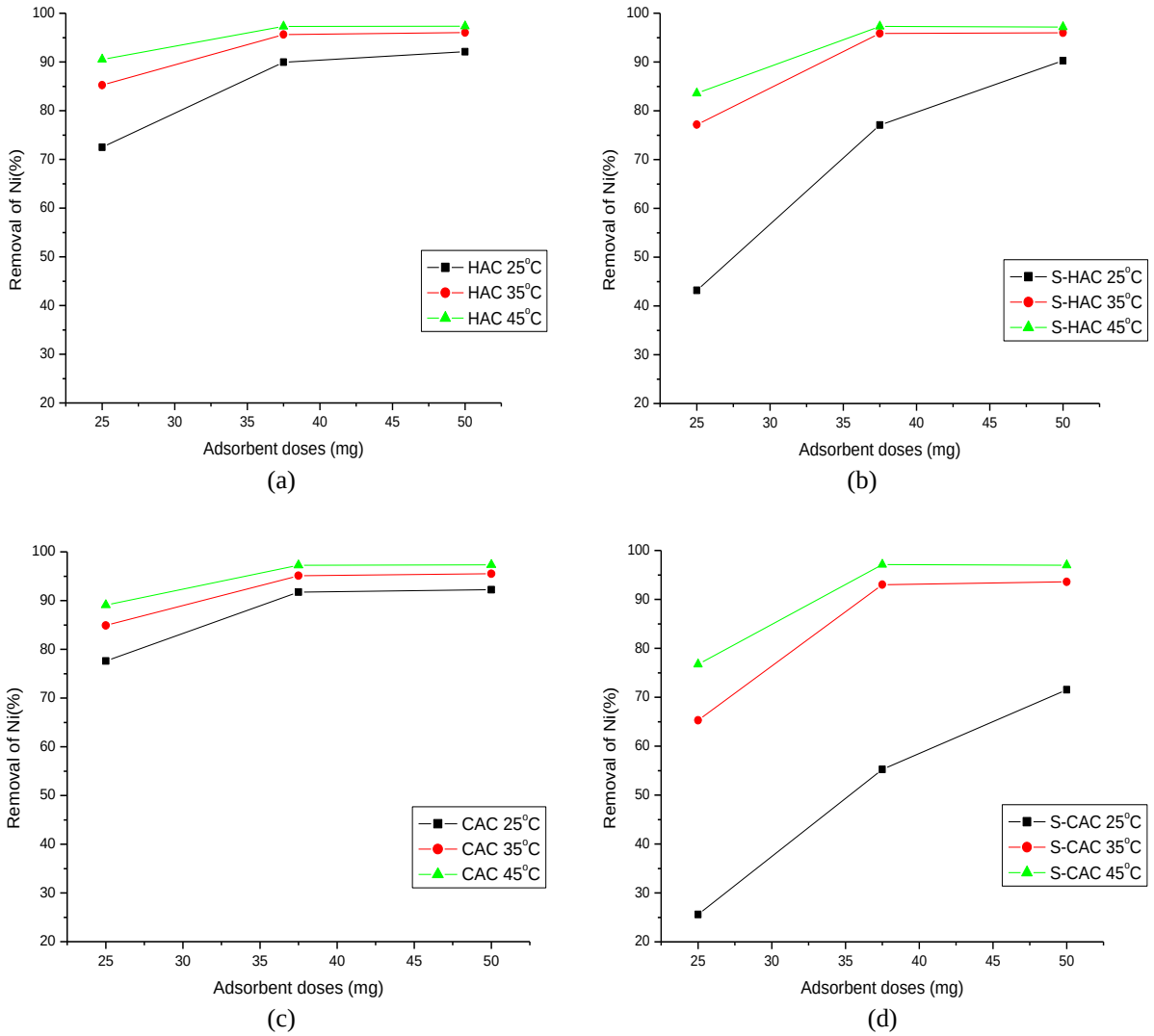

Figure 7. Effect of adsorbent doses and temperature on Ni removal % with C_0 Ni ions = 40 mg/L (a) HAC, (b) S-HAC, (c) CAC, (d) S-CAC, (V = 50 mL, initial pH = 6, final pH = 7.9-8.6, shake speed 50 rpm, t = 24 h, particle size class >0.063 mm).

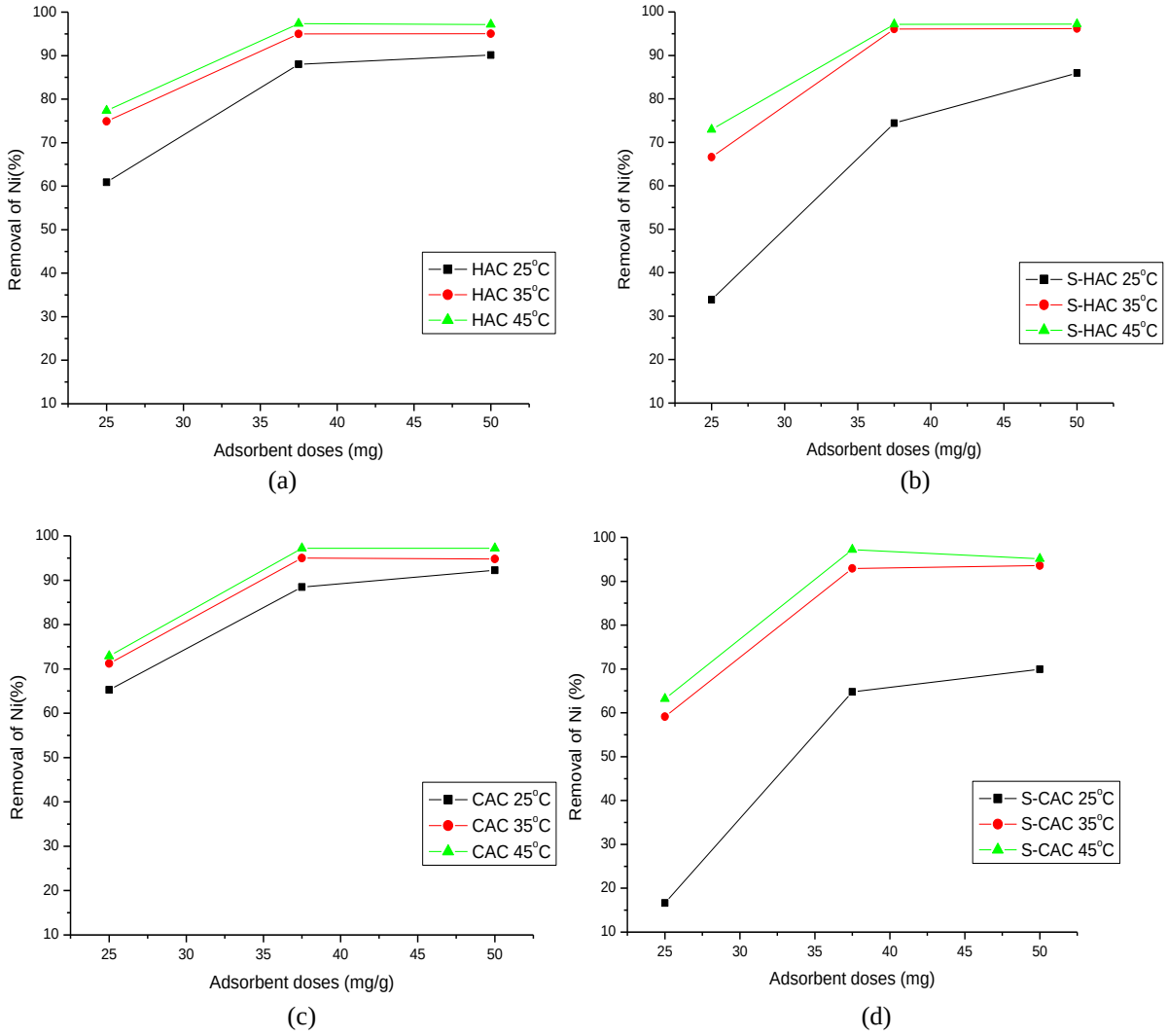

Figure 8. Effect of adsorbent doses and temperature on Ni % removal for a mixed Ni and Co solution (a) HAC, (b) S-HAC, (c) CAC, (d) S-CAC (C_0 Ni = 40 mg/L, C_0 Co= 5 mg/L V = 50 mL, initial pH = 6, final pH = 7.6 - 8.7, shake speed 50 rpm, t = 24 h, particle size class >0.063 mm).

3.6. Thermodynamic and kinetic parameters

Table 8 evidences the approximate thermodynamic parameters (according Equations 5 and 15, and reference 59) involved in the adsorption of Ni and Co in single ion solutions when the temperature was increased from 25ºC (298 K) up to 45ºC (318 K). Considering the error for the assumption of a dilute solution and neglecting ionic strength in using Liu approximation [59] in the estimation of K_{eq}, ΔH^o is positive and ΔG^o is negative. The adsorption of the metallic ion species has thus an endothermic and spontaneous nature. The ΔG^o becomes gradually more negative when the temperature increased from 25 to 45ºC, which demonstrates that the adsorption process is more favoured at higher temperatures (Figures 5-6). The ΔH^o determination gives different values depending on the equation used for K_{eq} estimation (Equations 5 and 15). Based on K_a (Equation. 15) ΔH^o values are higher for HAC and CAC compared to S-HAC and S-CAC values for both Ni and Co. Based on K_L (Equation. 5) this tendency was only found for Ni using HAC and S-HAC, for Co always the reverse was found. In all cases ΔH^o values are higher than 20 kJ/mol, pointing more to a chemical bonding process [59].

Table 7. Removal % for Co ions on Ni plus Co solution (C_o for Co = 5 mg/L, C_o for Ni = 40 mg/L m = 37.5 mg, pH = 6, V=50 mL, shake speed 50 rpm, t = 24 h).

Temperature 25°C		
Adsorbent Material	Ce (mg/L)	Removal %
HAC	0.267	94.48
CAC	0.114	97.11
S-HAC	0.423	91.79
S-CAC	1.017	81.57
Temperature 35°C		
HAC	< 0.10	> 98.93
CAC	< 0.10	> 98.93
S-HAC	< 0.10	> 98.93
S-CAC	< 0.10	> 98.93
Temperature 45°C		
HAC	< 0.10	> 98.93
CAC	< 0.10	> 98.93
S-HAC	< 0.10	> 98.93
S-CAC	< 0.10	> 98.93

Table 8. Thermodynamic parameters for ACs.

	Ni					Co				
	$\Delta H°$	$\Delta S°$	$\Delta G°$ kJ/mol			$\Delta H°$	$\Delta S°$	$\Delta G°$ kJ/mol		
	kJ/mol	J/molK	25ºC	35ºC	45ºC	kJ/mol	J/molK	25ºC	35ºC	45ºC
Based *Ka* (Eq. 15)										
HAC	30.32	178.99	-23.04	-24.77	-26.62	47.98	230.95	-21.02	-22.76	-25.67
CAC	34.28	193.27	-23.14	-25.62	-26.98	65.27	290.02	-21.40	-23.52	-27.23
S-HAC	23.24	148.30	-21.03	-22.28	-24.01	28.00	162.96	-20.70	-21.90	-23.98
S-CAC	32.18	173.02	-19.50	-20.84	-22.98	55.35	258.11	-21.80	-23.65	-27.00
Based K_L (Eq. 5) (after multiplying with 1000 and with the atomic weight of Ni or Co [59]										
HAC	74.73	331.45	-23.86	-27.73	-30.47	38.88	205.24	-22.45	-23.98	-26.58
CAC	37.04	205.67	-24.02	-26.77	-28.11	50.46	243.08	-22.11	-24.12	-26.99
S-HAC	65.18	287.59	-21.13	-22.08	-26.97	39.33	198.24	-19.99	-21.21	-23.99
S-CAC	47.66	225.96	-20.11	-21.01	-24.69	57.70	263.17	-21.29	-22.12	-26.64

The kinetics study was also performed for Ni in single and combined elemental solutions (Ni and Co) according with their concentration in the wastewater for an industrial acid leaching process. Figure 9 shows that the increment of temperature favours the adsorption kinetics of Ni ions. The equilibrium at 25ºC is reached very fast for HAC within 1 hour and for S-HAC within 2 h of contact time, while it takes 3 h for CAC and even 5 h for S-CAC. At higher temperatures (35 and 45ºC) the equilibrium time reached is again faster and is, like for HAC, again within 1 hour and for all others within 2 h. Kinetics of Co ion on combined elemental solutions (Figure 10) at low concentration (5 mg/L) occur also very rapidly achieving equilibrium even within 2 h at 35 and 45ºC for all studied adsorbents. At 25°C it takes 2 h for HAC and S-HAC, but 3 h for CAC and S-CAC. During kinetic processes the pH increases from 6 to values between 8.0-8.5 after 5 h of contact time.

The difference in kinetic behaviour seems to be related with surface functionalities, as the increment of q_{tNi} is more sharply for HAC and CAC at 25°C than for S-HAC and S-CAC. At 35 and 45°C the difference in q_{tNi} is less pronounced and thus in agreement with temperature effect results (Figures 5-6). As stated in section 3.4 with the increment of temperature, the role of surface functionalities seems to decrease in favour of an improved accessibility into the AC structure with better pore development and higher surface area for the Na_2S treated ACs. In addition, the mesopores play an important role providing the degree of accessibility to the micropores, in this case the ACs with higher contribution of mesopores (HAC and S-HAC) adsorb faster than CAC and S-CAC (Table 5). Also, the granulometric characteristics of adsorbent materials could be a key parameter in the equilibrium time. The adsorbent size distribution for AC based on coffee husks is mainly among 1-0.5 mm but AC from cocoa husks is mostly between 2-1 mm (Table 1), this increases the diffusion path length of the ions to achieve the adsorption sites.

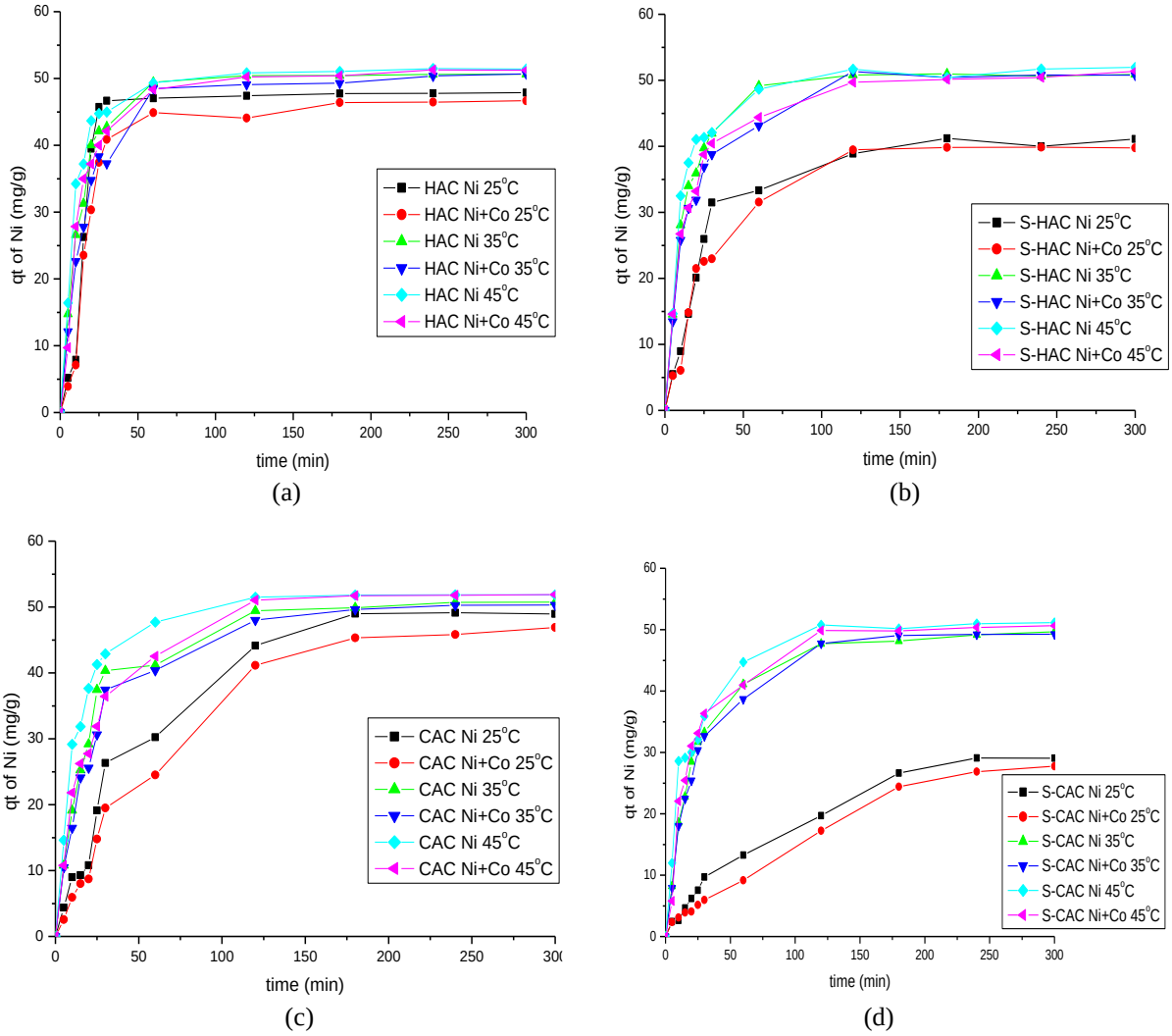

Figure 9. Adsorption kinetics of single Ni and mixed Ni and Co solutions (a) HAC, (b) S-HAC, (c) CAC, (d) S-CAC (m=37.5 mg, C_0 Ni = 40 mg/L, C_0 Co = 5 mg/L V = 50 mL, initial pH = 6, final pH = 8.0-8.5, shake speed 50 rpm, particle size class >0.063 mm).

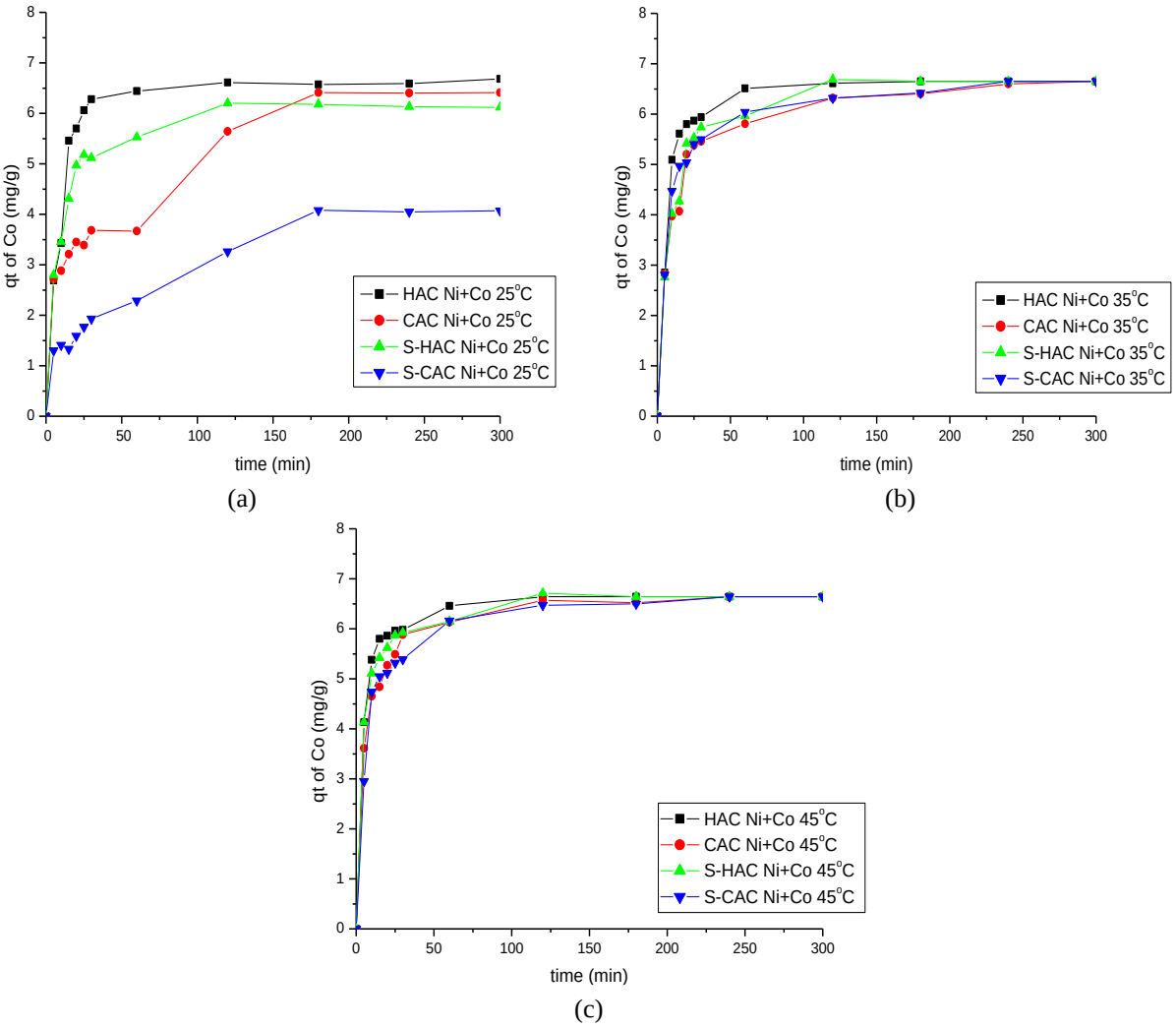

Figure 10. Adsorption kinetics of Co from Ni+Co solution (a) 25°C, (b) 35°C, (c) 45°C (m = 37.5 mg, C_0 Ni = 40 mg/L, C_0 Co = 5 mg/L V = 50 mL, pH = 6, shake speed 50 rpm).

Kinetics parameters for Ni ions in single and combined elemental solutions (Ni and Co) were obtained by fitting kinetic data with pseudo-first and pseudo-second order models (Table 9). HAC, CAC, S-HAC and S-CAC show very good agreements with pseudo-second order model for temperatures at 35 and 45°C, as well for single as for combined metal ion solutions. For both single and combined ion solutions at 25 °C nor pseudo-first nor pseudo-second kinetics gives real acceptable correlation coefficients, the reason for this is unclear. For S-HAC at 25°C pseudo-second order model for single Ni and combined solutions demonstrate a good to acceptable correlation value. However for CAC in combined ion solution similar fitting results are obtained for both pseudo-first and pseudo-second order model and an acceptable correlation coefficient for single Ni ion solution following the pseudo-second order model. In the case of S-CAC at 25°C in the single metal ion solution similar fitting results are obtained for both pseudo-first and pseudo-second order model. Pseudo-second order fittings for Ni ions in single solution are shown in Figure 11. The rate of adsorption is always in the order HAC > S-HAC >> CAC > S-CAC. The chemical pre-treatment reduces the rate of adsorption. The higher the temperature the smaller the difference in rate is for the first three adsorbents. The rate of adsorption clearly increased as a function of temperature, this is more pronounced for the single metal than for the bi-metal ion solution.

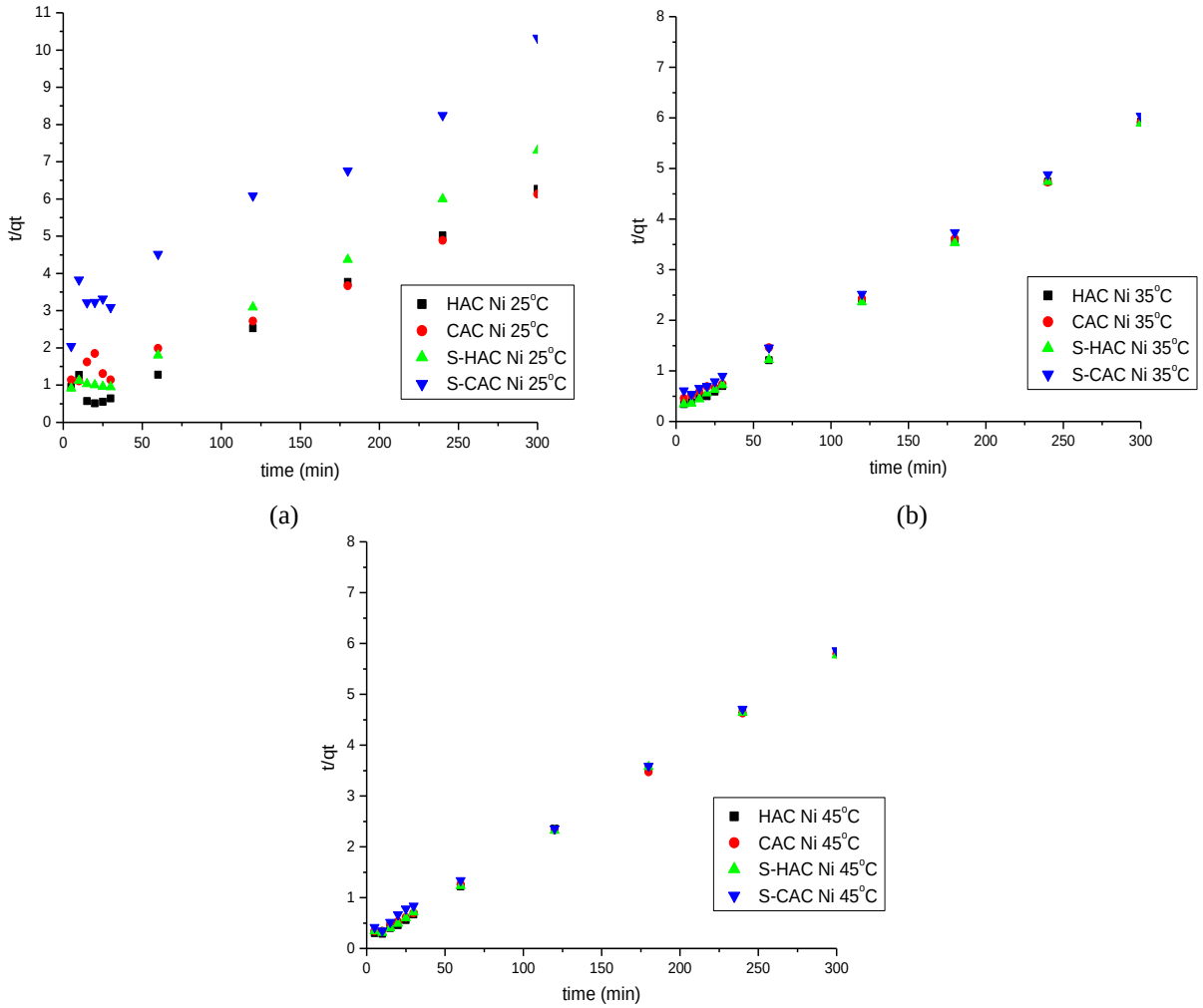

Figure 11. Pseudo-second order fitting for Ni solution (a) 25°C, (b) 35°C, (c) 45°C (m = 37.5 mg, C_0 Ni = 40 mg/L, V = 50 mL, pH = 6, shake speed 50 rpm).

Obtained Figure 9d for S-CAC at 25°C shows also a totally different global adsorption trend compared to the other Figures 9a-c. This could possibly be explained by the lower amount of oxygen surface functionalities as is determined via Boehm titration and XPS results (Table 4), which are decisive in the adsorption process at low temperature. The best fit by the pseudo-second order model suggests that the rate-limiting step could be chemisorption promoted either by covalent forces, through sharing or exchanging electrons. This mechanism of adsorption is improved with the increase of temperature. However, lower k_2 values are achieved for CAC and S-CAC. Based on Table 5, for CAC and S-CAC, the V_{Mes}/V_T ratios are the lowest, compared with HAC and S-HAC where V_{Mes}/V_T ratios are the highest. These results confirm that both surface functionalities and contribution of mesopores affect the kinetics behaviour.

In order to measure the impact of the diffusion process (through bulk solution, film boundary or intra-particle concept), a series of agitation and particle size variation experiments were done at 25°C. As agitation decreases the thickness of boundary layer diffusion and smaller particle size decreases the length path for diffusion through pores in the adsorbent, a change in the plots of qt vs time should be expected if diffusion process is an important rate controlling step [68]. Figures 12-13 show the kinetics performance of Ni in single and bi-elemental solutions (Ni and Co) at different agitation speed (50, 75 and 100 rpm; for

adsorbent size particles within the range 0.063-2 mm) and granulometric size (1-2 mm, 0.5-1 mm and 0.5-0.125 mm; all at 50 rpm) of adsorbent materials. For all adsorbents, the kinetic behaviour of Ni ions at different shake speed remains almost identical within the studied agitation speed 50-100 rpm (Figure 12). In the case of particle size, when smaller particle size is used in the adsorption process, only for CAC and S-CAC a faster increment in q_t during an intermediate period between 25-50 min and the first 200 minutes could be observed (Figure 13), which was not that obvious for HAC and S-HAC, however equilibrium time did not change.

Table 9. Kinetic parameters for ACs at different temperatures.

Carbon	*Ni (single solution)*				*Ni -Co solution*			
	Pseudo-first order		*Pseudo-second order*		*Pseudo-first order*		*Pseudo-second order*	
				At 25 ºC				
HAC	R^2	*0.6368*	R^2	*0.9730*	R^2	*0.8157*	R^2	*0.9658*
	k_1	*0.0140*	k_2	*9.9E-04*	k_1	*0.0140*	k_2	*7.2E-04*
CAC	R^2	*0.9104*	R^2	*0.9748*	R^2	*0.9884*	R^2	*0.9628*
	k_1	*0.0230*	k_2	*2.5E-04*	k_1	*0.0152*	k_2	*1.5E-04*
S-HAC	R^2	*0.8202*	R^2	*0.9932*	R^2	*0.8663*	R^2	*0.9850*
	k_1	*0.0175*	k_2	*8.4E-04*	k_1	*0.0244*	k_2	*6.7E-04*
S-CAC	R^2	*0.9624*	R^2	*0.9678*	R^2	*0.7829*	R^2	*0.7638*
	k_1	*0.0143*	k_2	*2.2E-04*	k_1	*0.0173*	k_2	*7.2E-05*
				At 35 ºC				
HAC	R^2	*0.7664*	R^2	*0.9993*	R^2	*0.9050*	R^2	*0.9991*
	k_1	*0.0134*	k_2	*2.5E-03*	k_1	*0.0157*	k_2	*1.7E-03*
CAC	R^2	*0.9540*	R^2	*0.9989*	R^2	*0.9493*	R^2	*0.9991*
	k_1	*0.0177*	k_2	*1.2E-03*	k_1	*0.015*	k_2	*9.7E-04*
S-HAC	R^2	*0.7719*	R^2	*0.9994*	R^2	*0.6817*	R^2	*0.9992*
	k_1	*0.0147*	k_2	*2.3E-03*	k_1	*0.0145*	k_2	*1.6E-03*
S-CAC	R^2	*0.9751*	R^2	*0.9990*	R^2	*0.9283*	R^2	*0.9985*
	k_1	*0.0168*	k_2	*9.9E-04*	k_1	*0.0159*	k_2	*8.9E-04*
				At 45 ºC				
HAC	R^2	*0.8067*	R^2	*0.9996*	R^2	*0.8471*	R^2	*0.9982*
	k_1	*0.0117*	k_2	*3.3E-03*	k_1	*0.0120*	k_2	*1.8E-03*
CAC	R^2	*0.8753*	R^2	*0.9995*	R^2	*0.9362*	R^2	*0.9991*
	k_1	*0.0175*	k_2	*2.1E-03*	k_1	*0.0193*	k_2	*1.1E-03*
S-HAC	R^2	*0.8752*	R^2	*0.9994*	R^2	*0.9200*	R^2	*0.9998*
	k_1	*0.0184*	k_2	*2.5E-03*	k_1	*0.0124*	k_2	*1.7E-03*
S-CAC	R^2	*0.8710*	R^2	*0.9991*	R^2	*0.9327*	R^2	*0.9938*
	k_1	*0.0136*	k_2	*1.4E-03*	k_1	*0.0170*	k_2	*9.4E-04*

According to Worch [69] the adsorption kinetics is determined by the main following stages: (1) transport of the adsorbate from the bulk liquid phase to the hydrodynamic boundary layer localized around the adsorbent particle, (2) transport through the boundary layer to the external surface of the adsorbent, (3) diffusion of molecules inside the pores, and (4) energetic interaction between the adsorbate molecules and the final adsorption sites. So even when the decrease of the particle size increases the surface contact between the adsorbate and

the adsorbent and the first two stages can be improved, the diffusion inside the pores depends on the mesoporous characteristics. The mesopores act as transport routes to reach the micropores, explaining why for CAC and S-CAC Ni ions reach slower the final adsorption locations than for HAC and S-HAC (V_{Mes}/V_T ratios are the highest). However, it is clear that the Ni ion uptake is more sensitive to the increment of temperature (Figure 9) than with the variation of agitation speed or adsorbent granulometric size (Figures 12-13). As a conclusion, for all ACs kinetics, the mechanism is rather controlled by chemisorption characteristics.

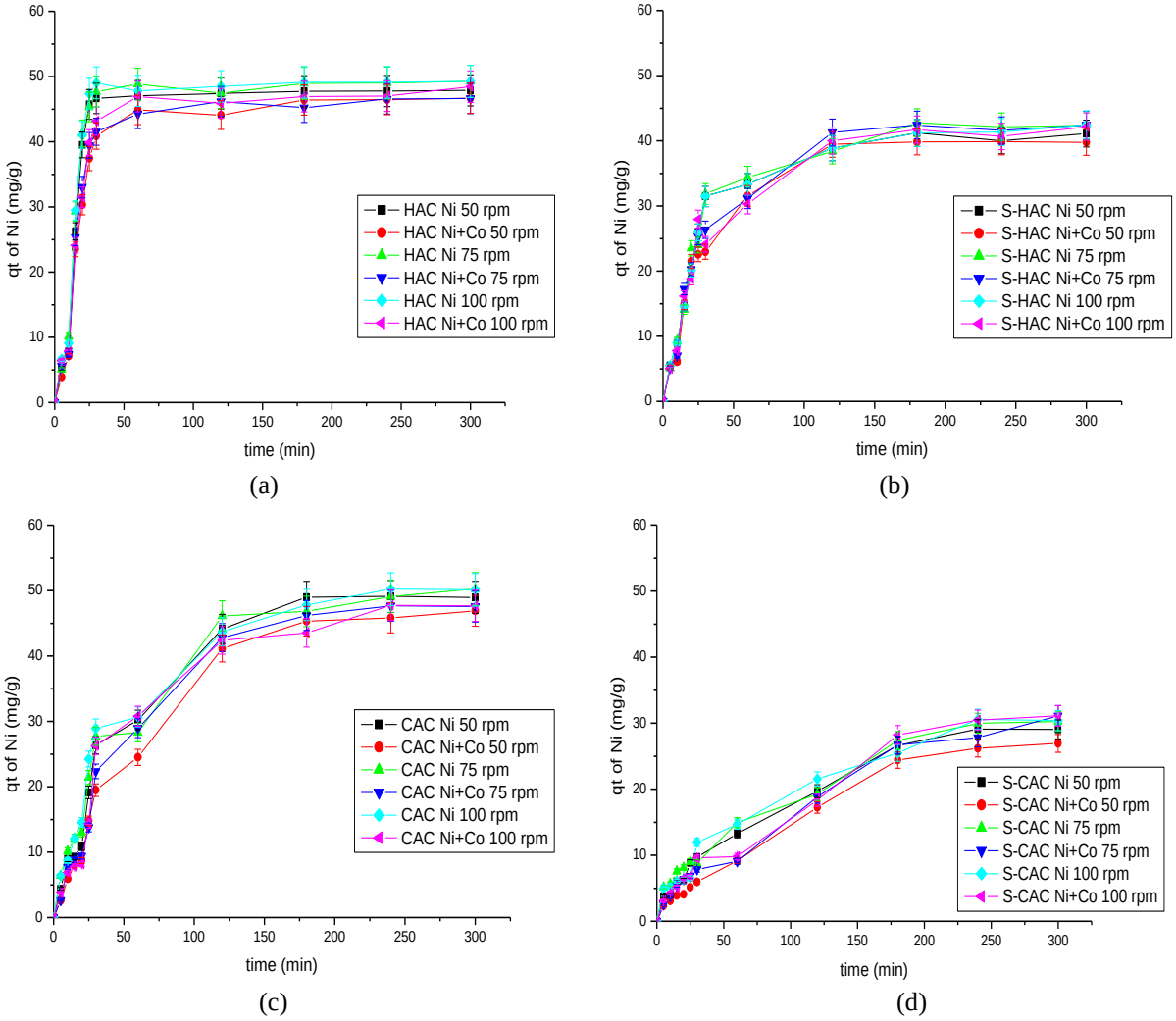

Figure 12. Adsorption kinetics at different shake speed (a) HAC, (b) S-HAC, (c) CAC, (d) S-CAC (m = 37.5 mg, C_0 Ni = 40 mg/L, C_0 Co = 5 mg/L V = 50 mL, initial pH = 6, final pH = 8.0-8.5, T = 25 ºC, particle size class >0.063 mm).

3.7. Activation energy results

The activation energy (E_a) for Ni ion adsorption obtained by fitting ln k_2 (as the pseudo-second order model is to be preferred) vs 1000/T for the single element solution system is presented in Table 10, including the estimated errors. In spite of the low correlation value of Arrhenius's equation (<0.95), an activation energy value for Ni adsorption is for all ACs greater than 30 kJ/mol which rather confirms that the controlling step is chemisorption and not physisorption [68, 70, 71], which is strongly dependent on temperature. For S-HAC the E_a (43.6 kJ/mol) minus the error (20.2) gives 23.4 kJ/mol, but with a low correlation coefficient value and considering the thermodynamic (Table 8) and the pseudo-second order kinetic model results (Table 9), it is possible to keep the chemisorption controlling step. As

varying agitation speed and adsorbent granulometric size (Figures 12-13) have little effect on the Ni ion uptake, the kinetic behaviour is explained by a "surface enhancement" and thus a possible increased number of adsorption sites [68].

The E_a order is: CAC > S-CAC > HAC > S-HAC, which is the inverse of the V_{Mes}/V_T ratio order consistent with the more difficult accessibility of the final adsorption sites. There is no relation between E_a order and the total amount of acidic groups (Table 3): CAC >HAC >S-HAC >S-CAC nor with the S_{BET} surface area order (Table 4): S-CAC > S-HAC > HAC > CAC.

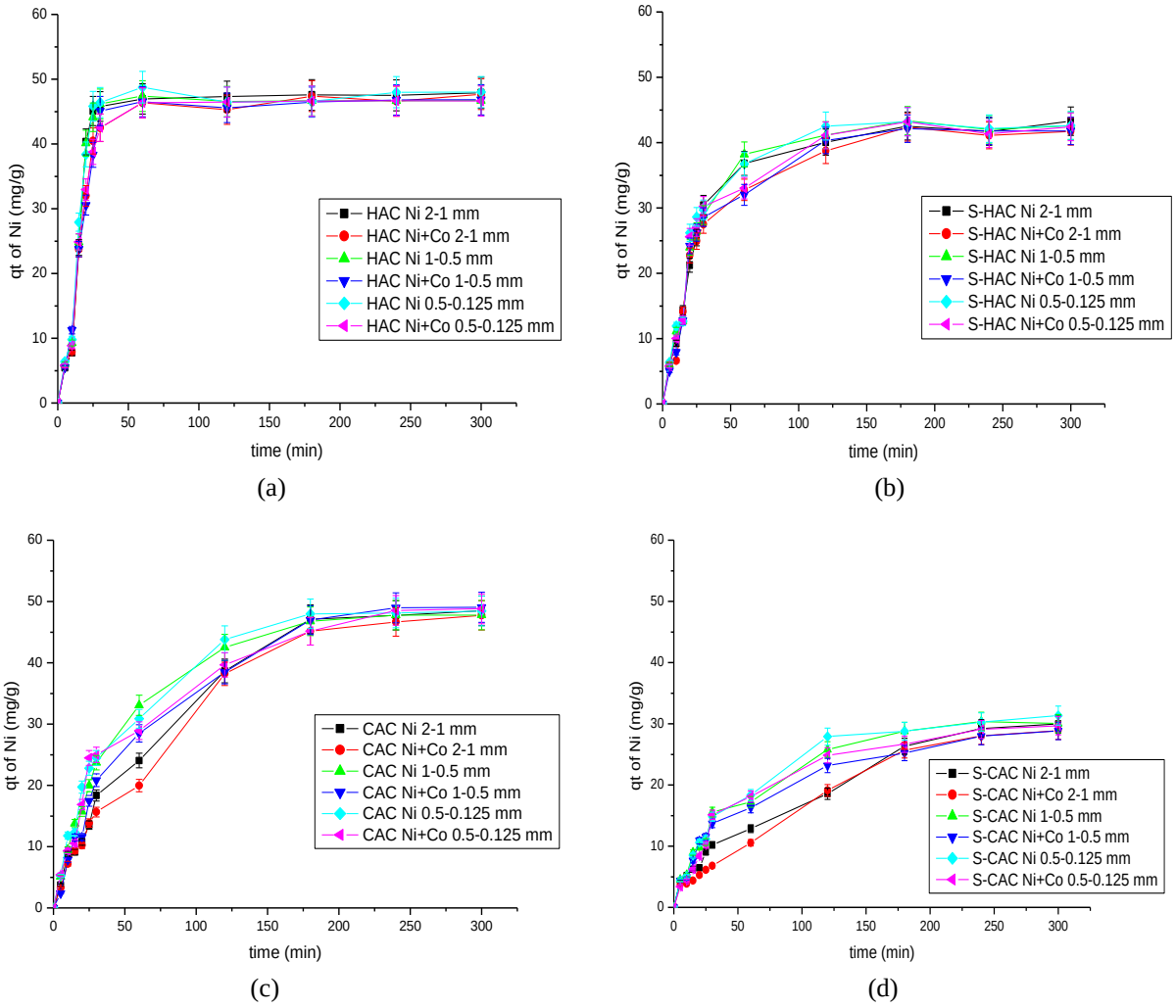

Figure 13. Adsorption kinetics at different granulometric size (a) HAC, (b) S-HAC, (c) CAC, (d) S-CAC (m = 37.5 mg, C_0 Ni = 40 mg/L, C_0 Co = 5 mg/L V = 50 mL, initial pH = 6, final pH = 8.0-8.5, T = 25 ºC, shake speed 50 rpm).

Table 10. Parameters from Arrhenius equation.

Carbon	Arrhenius equation parameters		
	E_a (kJ/mol)	A	R^2
HAC	48.3±13.4	3.22E+05	0.9285
CAC	84.7±21.3	2.06E+11	0.9409
S-HAC	43.6±20.2	4.26E+04	0.8238
S-CAC	57.8±25.9	4.96E+06	0.9184

3.8. Roll of the mineral matter in the adsorption mechanism

It is known that the presence of inorganic impurities in AC, leached during adsorption process, could affect its adsorption behaviour [72]. Table 11 shows the content (%) of Na, K, Ca and Mg in the adsorbents and in the solution after the adsorption process, using ACs with and without 0.1 N HCl leaching process. The ACs, pre-treated with Na_2S solution, show an increase in Na due to this treatment and the milli-Q washing procedure additional resulting in a strong decrease in K content and a slight decrease in Ca and Mg. After adsorption tests with Ni and Co most of the K and Na present in the carbon are released and thus exchanged with both metal ions. For Ca and Mg less exchange takes place (Table 11). In other words, an adsorption mechanism can also partly be proposed through ionic exchange.

In order to clarify if ionic exchange is important in adsorption mechanism, the ACs were subjected to a leaching process with a 0.1 N HCl solution during 48 h and washed with Milli-Q water until no significant changes is solution pH is observed. After being dried at 110ºC, the AC materials were used for a new adsorption test at the following conditions: 37.5 mg, 50 mL, 45ºC, pH = 6 in Ni plus Co solution with initial concentration at 40 mg/L and 5 mg/L respectively. After leaching the ACs with 0.1 N HCl solution, the content of Na and K in AC matrix is <0.05 %, the Ca and Mg are present in concentrations between 0.23 - 0.78 % and 0.18 - 0.48 %, respectively. Only for HAC and S-HAC Mg is still released towards the solution, but its content is lower than 0.1 %, evidencing that most of the Na, K, Ca and Mg are already leached during the pre-treatment with 0.1 N HCl solution. However, in all cases, using ACs with and without 0.1 N HCl leaching process, the removal % for Ni and Co ions were similar to the one achieved in the Figures 7-8, > 97 % of Ni(II) and > 98 % of Co(II), meaning that the content of Na, K, Ca and Mg does not have any impact on the adsorption process.

Table 11. Na, K, Ca and Mg content (%) in AC and solution after adsorption process at 45ºC.

Carbon	Metallic species present in the AC				Metallic species present in the solution after			
	Na %	K %	Ca %	Mg %	Na %	K %	Ca %	Mg %
HAC[a]	0.09	5.74	5.64	1.43	0.07	5.19	0.89	0.19
CAC[a]	0.19	7.32	2.83	2.11	0.13	6.06	0.17	0.48
S-HAC[a]	1.37	2.79	5.45	1.07	0.95	2.06	0.94	0.22
S-CAC[a]	2.13	4.44	2.58	2.04	1.12	2.96	0.22	0.69
HAC[b]	<0.05	<0.05	0.78	0.21	<0.05	<0.05	<0.05	0.09
CAC[b]	<0.05	<0.05	0.39	0.48	<0.05	<0.05	<0.05	<0.05
S-HAC[b]	<0.05	<0.05	0.64	0.18	<0.05	<0.05	<0.05	0.07
S-CAC[b]	<0.05	<0.05	0.23	0.26	<0.05	<0.05	<0.05	<0.05

[a]: AC without 0.1 mol/L HCl leaching process, [b]: AC previously leached with 0.1 mol/L HCl solution

3.9. Adsorption of Ni and Co ion in multi-element solution

Adsorption tests in a multi-element solution were performed simulating the concentration of metal ions in the wastewater from the industrial acid leaching process: 40 mg/L of Ni(II), 5 mg/L of Co(II), 1062 mg/L of Mg(II) and 1858 mg/L of Mn(II). The experiments were carried out at 45ºC (temperature selected according to the better results in single and combined solution mode tests) at different adsorbent doses and shown in Table 12. The affinity of studied ACs for metal ion uptake follows the order: Ni(II)>Co(II)>Mn(II)>Mg(II). Adsorption tests were performed for 1.25 and 2.5 g/L adsorbent dose.

Improved removal for Ni(II) of 12.8% and for Co(II) of 4.4% was measured for S-HAC compared to HAC in the presence of Mn(II) and Mg(II) using 1.25 g/L. Almost no improved adsorption of Mg(II) and Mn(II) could be noticed for S-HAC compared to HAC. In contrast, for S-CAC an increase in the removal of Mn(II) with 11.7% is found and for Mg(II) an almost 3.7% increase is noticed compared to CAC. However no improved adsorption for Ni(II) could be measured. In contrast, for Co(II) an almost comparable removal increase of 2.8% could be detected for Co(II) as found for S-HAC but still less than half what is found for S-HAC.

At adsorbent doses of 2.50 g/L the final solution pH increased to a value > 9.0 when HAC and CAC is used, causing a precipitation of heavy metal ions and diminishing the real value of q_e and removal (%). The removal % and adsorption capacities shown in Table 12 under this condition where adjusted for the amount of metal ions that precipitated. The increase in pH is a drawback compared to S-HAC and S-CAC. S-HAC demonstrates a removal % of Ni(II) and Co(II) of 69.27 and 48.68 % respectively without an increase in pH, exceeding far the 38.83 and 27.49 % achieved with S-CAC respectively. S-HAC seems therefore more interesting for the adsorption/removal of Ni(II) and Co(II). However for S-HAC and S-CAC also a substantial increase in removal % for Mn can be observed of 6.8% and 9.3% respectively. For Mg a much smaller increase removal % can be conducted of only 1.2 and 2.1% respectively.

The Ni and Co removals follow the order: S-HAC > HAC > S-CAC > CAC at adsorbent doses of 2.50 g/L, the same order as the mesoporosity development order (V_{Mes}/V_T ratio) and inversely to the E_a order found for Ni ion. These results prove that the Na_2S pre-treatment has a positive effect in the removal of Ni and Co in the presence of high amounts of Mg and Mn in industrial wastewaters. Additionally S-HAC and S-CAC allow the recovery of Ni(II) and Co(II) ions at higher adsorbent doses without heavy metal precipitation, which is in view of industrial application also interesting.

Table 12. Adsorption results in multi-element solution.

Carbon	Adsorbent doses (g/L)	Final pH	Ni		Co		Mn		Mg	
			qe (mg/g)	R %	qe (mg/g)	R %	qe (mg/g)	R %	qe (mg/g)	R %
HAC	1.25	7.38	6.23	39.14	0.68	33.91	122.08	16.43	24.68	5.81
CAC		7.33	3.97	24.97	0.27	13.61	32.68	4.40	10.24	2.41
S-HAC		7.08	8.27	51.98	0.77	38.30	120.60	16.23	27.28	6.42
S-CAC		7.15	3.78	23.76	0.33	16.46	119.92	16.14	25.88	6.09
HAC	2.50	9.03	4.10	51.59	0.38	37.22	80.68	21.71	11.68	5.50
CAC		9.22	3.01	37.89	0.25	25.13	47.90	12.86	8.62	4.06
S-HAC		7.22	5.51	69.27	0.49	48.68	104.10	28.01	14.34	6.75
S-CAC		7.31	3.09	38.83	0.28	27.49	82.46	22.19	13.12	6.18

4. Conclusions

The role of surface chemistry and textural characteristics of ACs from coffee and cocoa seed husks in the adsorption of Ni and Co ions was studied. Chemical pre-treatment of ACs with Na_2S improved the adsorption performance at higher temperature more than the untreated ACs. The adsorption of the ionic species is endothermic and spontaneous in nature. Both surface functionalities and mesopore development affect the kinetics being a chemisorption process in nature. At low temperature, in single metal-ion-solution, the adsorption process is more related with surface functionalities. But, with the increment of temperature an improved accessibility into the structure of AC with high contribution of mesopores enhanced the

adsorption performance of ACs. At high dosage and in multi-element solutions containing Ni(II), Co(II), Mn(II) and Mg(II) ions, the adsorption of Ni and Co by S-HAC compared to HAC and S-CAC demonstrates an increased removal % for Ni and Co with low adsorption tendency increase for Mn and Mg and no precipitation of Ni and Co, being very interesting for industrial applications.

Acknowledgement

The authors would like to thank VLIR-UOS (Flemish Interuniversity Council for University Development Cooperation) project between Belgium and Cuba for providing funding and granting the support of the current research.

References

[1] V. Srivastava, C. H. Weng, V. K. Singh, Y. C. Sharma, Adsorption of Nickel Ions from Aqueous Solutions by Nano Alumina: Kinetic, Mass Transfer, and Equilibrium Studies. J. Chem. Eng. Data, vol 56, pp. 1414-1422, 2011.

[2] S. Mahdavi, Nano-TiO 2 modified with natural and chemical compounds as efficient adsorbents for the removal of Cd +2, Cu +2, and Ni +2 from water. Clean Techn. Environ. Policy, vol 18, pp. 81-94, 2016.

[3] A. Dhar Dwivedi, S. Prabha Dubey, M. Sillanpää, Y.-N. Kwon, C. Lee, Distinct adsorption enhancement of bi-component metals (cobalt and nickel) by Fireweed-derived carbon compared to activated carbon: Incorporation of surface group distributions for increased efficiency. Chem. Eng. J., vol 281, pp. 713-723, 2015.

[4] P. Senthil Kumar, S. Ramalingam, S. Dinesh Kirupha, A. Murugesan, T. Vidhyadevi, S. Sivanesan, Adsorption behavior of nickel(II) onto cashew nut shell: Equilibrium, thermodynamics, kinetics, mechanism and process design. Chem. Eng. J., vol 167, pp. 122-131, 2011.

[5] F. T. Ademiluyi, R. Nwanam, Effect of Process Parameters on the Single Adsorption of Zinc and Nickel ions Using Activated Carbon from Waste Nigerian Bamboo. Int. J. Eng. Appl. Sci., vol 3, pp. 2394-3661, 2016.

[6] A. Ahmadpour, M. Tahmasbi, T. Rohani Bastami, J. Amel Besharati, Rapid removal of cobalt ion from aqueous solutions by almond green hull. J. Hazard. Mater., vol 166, pp. 925-930, 2009.

[7] A. Sheikhhosseini, M. Shirvani, H. Shariatmadari, F. Zvomuya, B. Najafic, Kinetics and thermodynamics of nickel sorption to calcium-palygorskite and calcium-sepiolite: A batch study. Geoderma, vol 217-218, pp. 111-117, 2014.

[8] M. Wang, F. Hao, G. Li, J. Huang, N. Bao, L. Huang, Preparation of Enteromorpha prolifera-based cetyl trimethyl ammonium bromide-doped activated carbon and its application for nickel (II) removal. Ecotox. Environ. Safe., vol 104, pp. 254-262, 2014.

[9] WHO, Guidelines for drinking-water quality. 4th edition. In: Chemical Fact Sheets. World Health Organization, Geneva, 2011.

[10] M. Nadeem, A. Mahmood, S. A. Shahid, S. S. Shah, A.M. Khalid, G. McKay, Sorption of lead from aqueous solution by chemically modified carbon adsorbents. J. Hazard. Mater., vol 138, pp. 604-613, 2006.

[11] F.-S. Zhang, J. O. Nriagu, H. Itoh, Mercury removal from water using activated carbons derived from organic sewage sludge. Water Res., vol 39, pp. 389-395, 2005.

[12] A. M. Youssef, T. El-Nabarawy, S. E. Samra, Sorption properties of chemically activated carbons: 1. Sorption of cadmium (II) ions. Colloids Surf. A Physicochem. Eng. Asp., vol 235, pp. 153-163, 2004.

[13] H. Yanagisawa, Y. Matsumoto, M. Machida, Adsorption of Zn(II) and Cd(II) ions onto magnesium and activated carbon composite in aqueous solution. Appl. Surf. Sci., vol 256, pp. 1619- 1623, 2010.

[14] M. Ghasemi, M. Z. Khosroshahy, A. B. Abbasabadi, N. Ghasemi, H. Javadian, M. Fattahi, Microwave-assisted functionalization of Rosa Canina-L fruits activated carbon with tetraethylenepentamine and its adsorption behaviour toward Ni (II) in aqueous solution: Kinetic, equilibrium and thermodynamic studies. Powder Technol. Vol 274, pp. 362-371, 2015.

[15] M. Adib Yahya, Z. Al-Qodah, C. W. Zanariah Ngah, Agricultural bio-waste materials as potential sustainable precursors used for activated carbon production: A review. Renew. Sust. Energ. Rev., vol 46 pp. 218-235, 2015.

[16] M. Kilic, E. Apaydin-Varol, A. E. Pütün, Adsorptive removal of phenol from aqueous solutions on activated carbon prepared from tobacco residues: Equilibrium, kinetics and thermodynamics. J. Hazard. Mater. vol 189, pp.397-403, 2011.

[17] F. Ahmad, W. Mohd Ashri, Wan Daud, M. Azmier Ahmad, R. Radzi, using cocoa (Theobroma cacao) shell-based activated carbon to remove 4-nitrophenol from aqueous solution: Kinetics and equilibrium studies. Chem. Eng. J., vol 178, pp. 461- 467, 2011.

[18] M. Azmier Ahmad, N. Khabibor Rahman, Equilibrium, kinetics and thermodynamic of Remazol Brilliant Orange 3R dye adsorption on coffee husk-based activated carbon. Chem. Eng. J., vol 170, pp. 154-161, 2011.

[19] M. Azmier Ahmad, N. Khabibor Rahman, Equilibrium, kinetics and thermodynamic of Remazol Brilliant Orange 3R dye adsorption on coffee husk-based activated carbon. Chem. Eng. J., vol 170, pp. 154-161, 2011.

[20] M. C. Baquero, L. Giraldo, J. C. Moreno, F. Suárez-García, A. Martínez-Alonso, J.M.D. Tascón, Activated carbons by pyrolysis of coffee bean husks in presence of phosphoric acid. J. Anal. Appl. Pyrolysis vol 70, pp. 779-784, 2003.

[21] V. Minkova, M. Razvigorova, E. Bjornbom, R. Zanzi, T. Budinova, N. Petrov, Effect of water vapour and biomass nature on the yield and quality of the pyrolysis products from biomass. Fuel Proc. Technol., vol 70, pp. 53-61, 2001.

[22] Minkova V., Marinov S.P., Zanzi R., Bjornbom E., Budinova T., Stefanova M., et al., Thermochemical treatment of biomass in a flow of steam or in a mixture of steam and carbon dioxide. Fuel Proc. Technol., vol 62, pp. 45-52, 2000.

[23] A. Marcilla, S. Garcıa-Garcıa, M. Asensio, J.A. Conesa, Influence of thermal treatment regime on the density and reactivity of activated carbons from almond shells. Carbon, vol 38, pp. 429-440, 2000.

[24] M. Ahmedna, W. E. Marshall, A. A. Husseiny, R. M. Rao, I. Goktepe, The use of nutshell carbons in drinking water filters for removal of trace metals. Water Res., vol 38, pp. 1062-1068, 2004.

[25] M. Ahmedna, W. E. Marshall, R. M. Rao, Production of granular activated carbons from select agricultural by- products and evaluation of their physical, chemical and adsorption properties. Bioresource Technol. vol 71, pp. 113-123, 2000.

[26] KKH. Choy, J. P. Barford, G. McKay, Production of activated carbon from bamboo scaffolding waste-process design, evaluation and sensitivity analysis. Chem. Eng. J., vol 109, pp. 147-165, 2005.

[27] F. T. Ademiluyi, S. A. Amadi, Jacob N. Amakama, Adsorption and treatment of organic contaminants using activated carbon from waste Nigerian bamboo. J. Appl. Sci. Environ Manag., vol 13, pp. 39-47, 2001.

[28] J. N. Sahu, J. Acharya, B. C. Meikap, Optimization of production conditions for activated carbons from tamarind wood by zinc chloride using response surface methodology. Bioresour. Technol., vol 101, pp. 74-82, 2010.

[29] I. Lupul, J. Yperman, R. Carleer, G. Gryglewicz, tailoring of porous texture of hemp-stem-based activated carbon produced by phosphoric acid activation in steam atmosphere. J. Porous Mater., vol 22, pp. 283-289, 2015.

[30] P. Ariyadejwanich, W. Tanthapanichakoon, K. Nakagawa, S.R. Mukai,H. Tamon, Preparation and characterization of mesoporous activated carbon from waste tires. Carbon, vol 41, pp. 157-164, 2003.

[31] A. Bhatnagar, W. Hogland, M. Marques, M. Sillanpää, An overview of the modification methods of activated carbon for its water treatment applications. Chem. Eng. J., vol 219, pp. 499-511, 2013.

[32] A. Arami-Niya, W. M. Ashri Wan Daud, F. S. Mjalli, Comparative study of the textural characteristics of oil palm shell activated carbon produced by chemical and physical activation for methane adsorption. Chem. Eng. Res. Des., vol 89, pp. 657-664, 2011.

[33] B. Jiang, Y. Zhang, J. Zhou, K. Zhang, S. Chen, Effects of chemical modification of petroleum cokes on the properties of the resulting activated carbon. Fuel, vol 87, pp. 1844-1848, 2008.

[34] L. Lin, S.-R. Zhai, Z.-Y. Xiao, Y. Song, Q.-D. An, X.-W. Song, Dye adsorption of mesoporous activated carbons produced from NaOH-pretreated rice husks. Bioresour. Technol., vol136 pp. 437-443, 2013.

[35] I. Lupul, J. Yperman, R. Carleer, G. Gryglewicz, Adsorption of atrazine on hemp stem-based activated carbons with different surface chemistry, Adsorption, vol 21, pp. 489-498, 2016.

[36] M. Carrier, H. W. Neomagus, J. Görgens, J. H. Knoetze, Influence of Chemical Pretreatment on the Internal Structure and Reactivity of Pyrolysis Chars Produced from Sugar Cane Bagasse. Energy Fuels, vol 26, pp. 4497−4506, 2012.

[37] Z. Hu, M. P. Srinivasan, Y. Ni, Preparation of Mesoporous High-Surface-Area Activated Carbon. Adv. Mater., vol 12, pp. 62-65, 2000.

[38] S. B. Lyubchik, R. Benoit, F. Beguin, Influence of chemical modification of anthracite on the porosity of the resulting activated carbons. Carbon, vol 40, pp. 1287-1294, 2002.

[39] T. Cornelissen, J. Yperman, G. Reggers, S. Schreurs and R. Carleer, Flash co-pyrolysis of biomass with polylactic acid. Part I: influence on bio-oil yield and heating value, Fuel, vol 87, pp. 1031-1041, 2008.

[40] M. Hernández Rodríguez, J. Yperman, R. Carleer, J. Maggen, S. Vanderheyden, J. Falcón Hernández, Alexis Otero Calvis, G. Gryglewicz, Evaluation of activation parameters on coffee and cocoa seed husk rest streams and Ni(II) adsorption capacity study on their activated carbon, Desalin. Water Treat., vol 104, pp. 175-188, 2018.

[41] F. Stoeckil, E. Daguerre, A. Guillot, The development of micropore volumes and widths during physical activation of various precursors, Carbon, vol 37, pp. 2075-2077, 1999.

[42] A.V. Neimark, Y. Lin, P.I. Ravikovitch, M. Thommes, Quenched solid density functional theory and pore size analysis of micro-mesoporous carbons, Carbon, vol 47, pp. 1617-1628, 2009.

[43] F. Stoeckli, M. V. Lopez-Ramon, C. Moreno-Castilla, Adsorption of phenolic compounds from aqueous solutions, by activated carbons, described by the Dubinin-Astakhov equation, Langmuir, vol 17, pp. 3301-3306, 2001.

[44] P. Tarazona, M. Bettolo Marconi., R. Evans, Phase equilibria of fluid interfaces and confined fluids: non-local versus local density functionals, Mol. Phys., vol 60, pp. 573, 1987.

[45] P. C. C. Faria, J. J. M. Orfao, M. F. R. Pereira, Adsorption of anionic and cationic dyes on activated carbons with different surface chemistries, Water Res., vol 38, pp. 2043-2052, 2004.

[46] H. P. Boehm, Some aspects of the surface-chemistry of carbon-blacks and other carbons, Carbon, vol 32, pp. 759-769, 1994.

[47] ASTM 1756-01, Standard Test Method for Determination of Total Solids in Biomass. ASTM International, West Conshohocken, 2001.

[48] ASTM D 3175-17, Standard Test Method for Volatile Matter in the Analysis Sample of Coal and Coke. ASTM International, West Conshohocken, 2017.

[49] ASTM E 1755-01, Standard Test Method for Ash in Biomass. ASTM International, West Conshohocken, 2015.

[50] W. E. Oliveira, A. S. Franca, L. S. Oliveira, S. D. Rocha, Untreated coffee husks as biosorbents for the removal of heavy metals from aqueous solutions, J. Hazard. Mater., vol 152, pp. 1073-1081, 2008.

[51] K.Y. Foo, B.H. Hameed, Insights into the modeling of adsorption isotherm systems, Chem. Eng. J., vol 156, pp. 2-10, 2010.

[52] S. Kundu, A. K. Gupta, Arsenic adsorption onto iron oxide-coated cement (IOCC): regression analysis of equilibrium data with several isotherm models and their optimization, Chem. Eng. J., vol 122, pp. 93-106, 2006.

[53] A. B. Pérez-Marín, V. Meseguer Zapata, J. F. Ortuno, M. Aguilar, J. Sáez, M. Llorens, Removal of cadmium from aqueous solutions by adsorption onto orange waste, J. Hazard. Mater. B, vol 139, pp. 122-131, 2007.

[54] K. R. Hall, L. C. Eagleton, A. Acrivos, T. Vermeule, Pore and solid-diffusion kinetics in fixed-bed adsorption under constant-pattern conditions, Ind. Eng. Chem. Fund., vol 5, pp. 212-223, 1966.

[55] M. El-Sadaawy, O. Abdelwahab, Adsorptive removal of nickel from aqueous solutions by activated carbons from doum seed (Hyphaenethebaica) coat, Alexandria Eng. J., vol 53, pp. 399-408, 2014.

[56] G. P. Jeppu, T. Prabhakar Clement, A modified Langmuir-Freundlich isotherm model for simulating pH-dependent adsorption effects, J. Contam. Hydrol. vol 129-130, pp. 46-53, 2012.

[57] M. A. Ahmad, N. K. Rahman, Equilibrium, kinetics and thermodynamic of Remazol Brilliant Orange 3R dye adsorption on coffee husk-based activated carbon, Chem. Eng. J., vol 170, pp. 154-161, 2011.

[58] L. S. Oliveira, A. S. Franca, T. M. Alves, S. D. F. Rocha, Evaluation of untreated coffee husks as potential biosorbents for treatment of dye contaminated waters, J. Hazard. Mater., vol 155, pp. 507-512, 2008.

[59] Yu Liu, Is the Free Energy Change of Adsorption Correctly Calculated? J. Chem. Eng. Data, vol 54, pp. 1981-1985, 2009.

[60] A. Kshama, Shroff, K.V. Varsha, Kinetics and equilibrium studies on biosorption of nickel from aqueous solution by dead fungal biomass of Mucor hiemalis. Chem. Eng. J., vol 171, pp. 1234-1245, 2011.

[61] M. A. Tofighy, T. Mohammadi, Adsorption of divalent heavy metal ions from water using carbon nanotube sheets, J. Hazard. Mater., vol 185, pp. 140-147, 2011.

[62] Z. Aksu, Determination of the equilibrium, kinetic and thermodynamic parameters of the batch adsorption of Ni(II) ions on to Chlorella vulgaris. Process Biochem., vol 38, pp. 89-99, 2002.

[63] S. N. do Carmo Ramos, A. L. Pedrosa Xavier, F. Simões Teodoro, L. Frédéric Gil, L. V. Alves Gurgel, Removal of cobalt(II), copper(II), and nickel(II) ions from aqueous solutions using phthalate-functionalized sugarcane bagasse: Mono- and multicomponent adsorption in batch mode. Ind. Crop. Prod., vol 79, pp. 116-130, 2016.

[64] J. Coates, Interpretation of Infrared Spectra, A Practical Approach, Encyclopedia of Analytical Chemistry, John Wiley & Sons, Ltd. 2006.

[65] M. Ghasemi, M.Z. Khosroshahy, A.B. Abbasabadi, N. Ghasemi, H. Javadian, M. Fattahi, Microwave-assisted functionalization of Rosa Canina-L fruits activated carbon with tetraethylenepentamine and its adsorption behaviour toward Ni (II) in aqueous solution: Kinetic, equilibrium and thermodynamic studies, Powder Technology, vol 274, pp. 362-371, 2015.

[66] M. A. Kader, M. R. Islam, M. Parveen, H. Haniu, and K. Takai, Pyrolysis decomposition of tamarind seed for alternative fuel. Bioresour. Technol., vol 149, pp. 1-7, 2013.

[67] M. Thommes, K. Kaneko, A. V. Neimark, J. P. Olivier, F. Rodriguez-Reinoso, J. Rouquerol, K. S.W. Sing, Physisorption of gases, with special reference to the evaluation of surface area and pore size distribution (IUPAC Technical Report). Pure Appl. Chem., vol 87, pp. 1051-1069, 2015.

[68] Y.S. Ho, J.C.Y. Ng, G. McKay, Kinetics of pollutant sorption by biosorbents: Review. Sep. Purif. Methods, vol 29, pp. 189-232, 2000.

[69] E. Worch, Adsorption Technology in Water Treatment. Fundamentals, Processes, and Modeling. Walter de Gruyter GmbH & Co. KG, Berlin/Boston, 2012.

[70] M. Danish, R. Hashim, M.N. Mohamad Ibrahim, M. Rafatullah, O. Sulaiman, T. Ahmad, M. Shamsuzzoha, A. Ahmad, Sorption of Copper(II) and Nickel(II) Ions from Aqueous Solutions Using Calcium Oxide Activated Date (Phoenix dactylifera) Stone Carbon: Equilibrium, Kinetic, and Thermodynamic Studies. J. Chem. Eng. Data, vol 56, pp. 3607-3619, 2011.

[71] A. Sheikhhosseini, M. Shirvani, H. Shariatmadari, F. Zvomuya, B. Najafic. Kinetics and thermodynamics of nickel sorption to calcium-palygorskite and calcium-sepiolite: A batch study. Geoderma, vol 217-218, pp. 111-117, 2014.

[72] T. J. Bandosz (Editor), Activated Carbon Surfaces in Environmental Remediation. Interface Science and Technology-Vol 7. 1st Edition, New York, 2006.